E-cadherin/ROS1 inhibitor synthetic lethality in breast cancer

Ilirjana Bajrami[1,2], Rebecca Marlow[3], Marieke van de Ven[4], Rachel Brough[1,2], Helen N. Pemberton[1,2], Jessica Frankum[1,2], Fei Fei Song[1,2], Rumana Rafiq[1,2], Asha Konde[1,2], Dragomir B. Krastev[1,2], Malini Menon[1,2], James Campbell[1,2], Aditi Gulati[1,2], Rahul Kumar[1,2], Stephen J. Pettitt[1,2], Mark D. Gurden[1], Marta Llorca Cardenosa[1,5], Irene Chong[1], Patrycja Gazinska[3], Fredrik Wallberg[6], Elinor J. Sawyer[7], Lesley-Ann Martin[1], Mitch Dowsett[1], Spiros Linardopoulos[1,8], Rachael Natrajan[1], Colm J. Ryan[9], Patrick W.B. Derksen[10], Jos Jonkers[11], Andrew N.J. Tutt[1,3], Alan Ashworth[12*], Christopher J. Lord[1,2*]

[1]The Breast Cancer Now Toby Robins Breast Cancer Research Centre and [2]CRUK Gene Function Laboratory, The Institute of Cancer Research, London, SW3 6JB, United Kingdom. [3]The Breast Cancer Now Research Unit, King's College London, London, United Kingdom. [4]Mouse Clinic for Cancer and Aging (MCCA) Preclinical Intervention Unit, The Netherlands Cancer Institute, Plesmanlaan 121, 1066 CX Amsterdam, The Netherlands. [5]Biomedical Research Institute INCLIVA, Hospital Clinico Universitario Valencia, University of Valencia, Spain. [6]FACS Core Facility, The Institute of Cancer Research, London, SW3 6JB, United Kingdom. [7]Division of Cancer Studies, Guy's Hospital, King's College London, London, SE1 9RT, United Kingdom. [8]Cancer Research UK Cancer Therapeutics Unit, Division of Cancer Therapeutics, The Institute of Cancer Research, London, United Kingdom. [9]Systems Biology Ireland, University College Dublin, Dublin 4, Ireland. [10]Department of Pathology, University Medical Center Utrecht, Heidelberglaan 100, 3584 CX Utrecht, The Netherlands. [11]Division of Molecular Pathology and Cancer Genomics Netherlands, The Netherlands Cancer Institute, Amsterdam, The Netherlands. [12]UCSF Helen Diller Family Comprehensive Cancer Centre, San Francisco, California 94158, USA.

Keywords. E-cadherin, ROS1, crizotinib, breast cancer, synthetic lethality

Additional information. This work was funded by a Programme Grant from Breast Cancer Now to CJL as part of their funding to the Breast Cancer Now Toby Robins Breast Cancer research Centre

***Corresponding authors:**

Prof. Christopher Lord, The Breast Cancer Now Toby Robins Breast Cancer Research Centre and CRUK Gene Function Laboratory, The Institute of Cancer Research, London, SW3 6JB, United Kingdom. Email Chris.Lord@icr.ac.uk

Prof. Alan Ashworth, UCSF Helen Diller Family Comprehensive Cancer Centre, San Francisco, California 94158, USA Email alan.ashworth@ucsf.edu

Conflict of interest disclosure statement. We have no conflicts to declare.

Total number of figures and tables = Seven Figures, 20 Supplementary Figures, 11 Supplementary Tables and five Supplementary Videos.

Abstract

The cell adhesion glycoprotein E-cadherin (*CDH1*) is commonly inactivated in breast tumours. Precision medicine approaches that exploit this characteristic are not available. Using perturbation screens in breast tumour cells with CRISPR-Cas9 engineered *CDH1* mutations, we identified synthetic lethality between E-cadherin deficiency and inhibition of the tyrosine kinase ROS1. Data from large-scale genetic screens in molecularly diverse breast tumour cell lines established that the E-cadherin/ROS1 synthetic lethality was not only robust in the face of considerable molecular heterogeneity but was also elicited with clinical ROS1 inhibitors including foretinib and crizotinib. ROS1 inhibitors induced mitotic abnormalities and multinucleation in E-cadherin defective cells, phenotypes associated with a defect in cytokinesis and aberrant p120-catenin phosphorylation and localisation. *In vivo,* ROS1 inhibitors produced profound anti-tumour effects in multiple models of E-cadherin defective breast cancer. This data therefore provides the pre-clinical rationale for assessing ROS1 inhibitors such as the licensed drug crizotinib in appropriately stratified patients.

Statement of significance

E-cadherin defects are common in breast cancer but are currently not targeted with a precision medicine approach. Our pre-clinical data indicate that licensed ROS1 inhibitors, including crizotinib, should be repurposed to target E-cadherin defective breast cancers, thus providing the rationale for the assessment of these agents in molecularly–stratified phase 2 clinical trials.

Introduction

E-cadherin defects are frequently found in breast cancer (>13 %) and gastric cancer (>14%) and are particularly prevalent in lobular breast cancers, which account for 15% of all mammary carcinomas (1). *CDH1* encodes a calcium-dependent plasma membrane-bound cell-cell adhesion glycoprotein (2). In epithelial cells, E-cadherin forms homotypic adhesive complexes, known as adherens junctions that control cell-cell contact, the contractility of cells and ultimately the integrity of epithelial cell layers (3). Whilst the extracellular domain of E-cadherin interacts with E-cadherin molecules on adjacent cells, the intracellular domain interacts with, and controls, a number of proteins including p120-catenin (p120), α-catenin, γ-catenin, β-catenin, receptor tyrosine kinases, and a series of plasma membrane-associated receptors and cytoskeletal proteins (2). Loss of E-cadherin function causes a wide variety of phenotypes ranging from defects in cell migration and the orientation of the mitotic spindle, as well as dysregulation of cell-cell adhesion and anoikis resistance (reviewed in (3)).

In lobular breast cancer, loss of E-cadherin expression occurs early on in the tumourigenic process and is seen in up to 90% of cases often co-occurring with mutations in the PI3-kinase coding gene, *PIK3CA* (4). Lobular breast cancers tend to be estrogen receptor (ER) and progesterone receptor (PR) positive, *ERBB2* amplification-negative, have a low Ki67 index and a luminal-A intrinsic subtype (1,5-7). Whilst these biomarkers might predict a favorable response to adjuvant endocrine therapy, retrospective analyses of two recent clinical trials (BIG 1-98 and ABCSG-8) suggests that a subset of invasive lobular breast cancer (ILC) patients have poorer responses to endocrine therapy when compared to those with invasive ductal carcinomas (IDCs) that display similar biomarkers (8,9). Furthermore, pathological complete response rates after neoadjuvant chemotherapy are low in ILC (10,11), suggesting that additional approaches are

required to target this disease. In other breast cancer subtypes, E-cadherin expression might also influence patient outcome. For example in triple negative breast cancer, the prognosis of patients with E-cadherin-negative tumours is significantly worse than those with E-cadherin-positive disease (12,13).

At present, it is not clear whether actionable or pharmacologically tractable E-cadherin synthetic lethal effects can be identified that are likely to work clinically. Such clinically actionable synthetic lethal effects might be expected to be relatively resilient to additional molecular changes and operate in the face of a high-degree of molecular diversity that exits in cancer (i.e. hard synthetic lethal effects (14)). In the data presented below, we illustrate that the combined use of multiple, distinct, *in vitro, ex vivo* and *in vivo* model systems and the exploitation of different functional profiling modalities (genetic and chemical screens) can be used to identify robust and actionable E-cadherin synthetic lethal interactions. The most notable synthetic lethality we identified in this way was between E-cadherin and the ROS1 receptor tyrosine kinase, an effect that is clinically actionable using ROS1 inhibitors such as crizotinib or foretinib.

Results

Integrated genetic and small molecule screens identify a ROS1/E-cadherin synthetic lethal effect

To identify candidate therapeutic targets for breast cancers with loss of E-cadherin, we used CRISPR-Cas9 mutagenesis in MCF7 breast tumour cells (ERα-positive, luminal A, *PIK3CA* mutant; described hereafter as $MCF7^{Parental}$ cells) to generate daughter clones, $MCF7^{A02}$, $MCF7^{B04}$ and $MCF7^{B05}$, with frameshift mutations in *CDH1* and loss of E-cadherin expression (Fig. 1A and B; Supplementary Fig. S1). Compared to $MCF7^{Parental}$ cells, E-cadherin defective cells displayed a rounded morphology also seen in breast tumour cells harbouring naturally occurring E-

cadherin mutations (Fig. 1C). We used $MCF7^{A02}$ and $MCF7^{Parental}$ cells in two parallel functional screens to identify E-cadherin synthetic lethal effects: (i) a drug sensitivity screen where we assessed the relative sensitivity of cells to an in–house curated library of 80 small-molecule inhibitors that are either in clinical use for the treatment of cancer or in late-stage clinical development (Fig. 1D; Supplementary Table S1 and S2); and (ii) a parallel siRNA sensitivity screen, using siRNA SMARTpools (four different siRNAs targeting a single gene in each well) targeting >1000 cell cycle control genes, kinase-coding genes or DNA repair related genes (see methods, Fig. 1E; Supplementary Table S3). The drug sensitivity screens identified a series of candidate E-cadherin synthetic lethal drugs, including PF-03758309 (a PAK inhibitor), PF-03814735 (an Aurora kinase inhibitor), PI3K/mTOR inhibitors (BEZ-235, PF-04691502 and Everolimus), the ROS1/MET/ALK inhibitors (15) crizotinib (PF02341066, Pfizer) and foretinib (GSK1363089, GSK) (Fig. 1D; Supplementary Table S1 and S2). In order to identify E-cadherin synthetic lethal effects from our MCF7 isogenic cell line siRNA screen, we calculated the difference in siRNA Z scores between E-cadherin defective and E-cadherin proficient cells and identified 104 E-cadherin synthetic lethal effects ($p < 0.05$, Fig. 1E; Supplementary Table S3). Gene ontology analysis of this 104 gene list using EnrichR (16) highlighted gene sets associated with myosin light chain kinase activity (Supplementary Table S4, adjusted *p*-value = 8.52×10^{-9}, PLK3, AAK1, HUNK, CSNK1A1, NEK4, PAK4, CPNE3, PIM1, CLK3, RPS6KA2, SBK1, STK38L, TGFBR1 and MYLK2), gene sets related to GTP-dependent protein kinase activity (Supplementary Table S4, adjusted *p*-value = 1.35×10^{-8}, PLK3, AAK1, HUNK, CSNK1A1, NEK4, PAK4, CPNE3 PIM1, CLK3, RPS6KA2, SBK1, STK38L, TGFBR1), and a set of candidate synthetic lethal genes associated with Rho-dependent protein serine/threonine kinase activity (Supplementary Table S4, adjusted *p*-value = 1.35×10^{-8}, PLK3, AAK1, HUNK, CSNK1A1, NEK4, PAK4, CPNE3, PIM1, CLK3, RPS6KA2, SBK1, STK38L, TGFBR1). Other gene sets identified in this analysis included genes associated with

RNA polymerase II carboxy-terminal domain kinase activity (Supplementary Table S4, adjusted *p*-value = 8.52E-09), protein serine/threonine kinase activity (Supplementary Table S4, adjusted *p*-value = 8.52×10^{-9}) and calmodulin-dependent protein kinase activity (Supplementary Table S4, adjusted *p*-value = 8.85×10^{-9}).

Amongst the most significant hits in the siRNA screen was ROS1 (ROS Proto-Oncogene 1, Receptor Tyrosine Kinase, Fig. 1E; Supplementary Table S3). We selected ROS1 for further study as: (i) the synthetic lethality observed with ROS1 siRNA was statistically significant; and (ii) the parallel small molecule inhibitor screen identified ROS1 inhibitors (foretinib, crizotinib) as candidate synthetic lethal drugs, suggesting that the ROS1 effect might be clinically tractable. The siRNA screen did not identify other targets of crizotinib or foretinib (e.g. KDR, MET, ALK and AXL) as being candidate E-cadherin synthetic lethal effects (Supplementary Fig. S2). We also noted that in both MCF7 and MCF10A isogenic systems, loss of E-cadherin expression caused upregulation of ROS1 protein but did not elicit changes in either MET or ALK expression (Fig. 1F,G; Supplementary Fig. S3), suggesting that enhanced ROS1 expression could represent a homeostatic response to E-cadherin loss; re-expression of E-cadherin in E-cadherin defective $MCF7^{A02}$ cells reversed this ROS1 induction (Fig. 1H), suggesting causality.

In validation experiments, we found that each of the four individual ROS1 siRNAs from the ROS1 SMARTpool caused silencing of ROS1 and preferentially inhibited the E-cadherin deficient $MCF7^{A02}$ clone and also an E-cadherin defective MCF10A $CDH1^{-/-}$ non-tumour cell line (Fig. 2A-C). Two further E-cadherin defective clones derived by MCF7 CRISPR-Cas9 targeting, $MCF7^{B04}$ and $MCF7^{B05}$, were also significantly more sensitive to either foretinib or crizotinib than the parental cells (Fig. 2D; Supplementary Fig. S1), suggesting these effects were not private to $MCF7^{A02}$. Restoring E-cadherin expression in $MCF7^{A02}$ using a Flag-epitope tagged E-cadherin

cDNA expression construct reduced foretinib sensitivity as well as sensitivity to an additional ROS1/MET/ALK inhibitor, TAE673 (Fig. 2E and F), confirming that E-cadherin influences the response to these agents. By assessing the effects of additional ROS1/MET/ALK inhibitors on E-cadherin isogenic cells, we found that foretinib and crizotinib gave the greatest difference in drug sensitivity between E-cadherin wild type and defective cells (Fig. 2G), warranting their further investigation. The sensitivity of E-cadherin defective cells to foretinib was similar to that observed in HCC78 cells (Fig. 2H and I), which harbour a *SLC34A2-ROS1* gene fusion rearrangement rendering the cell line highly addicted to ROS1 kinase activity (15). We also found E-cadherin defective cells to be sensitive to a recently described ROS1 kinase inhibitor, PF-06463922 (17) (Fig. 2J). Finally, transfection of E-cadherin defective $MCF7^{A02}$ cells with increasing amounts of ROS1 siRNA enhanced the cell inhibitory effects of foretinib (Fig. 2K). Conversely, expression of a crizotinib-refractory p.G2032R mutant *ROS1* fusion cDNA (18) caused crizotinib resistance in E-cadherin defective cells (Fig. 2L), suggesting that ROS1 could be a critical foretinib/crizotinib target in these cells.

Many synthetic lethal effects are private to a small number of model systems and do not operate universally in the face of the molecular diversity found in breast and other cancers (14). To assess whether the synthetic lethal effect of ROS1 inhibition could apply more widely in breast cancer with E-cadherin loss, we interrogated recently described in-house siRNA “Achilles’ Heel” screen data describing the kinase dependencies in 34 breast tumour cell lines (19). We first determined the E-cadherin protein expression in each of these 34 models by western blotting, classifying cell lines as either “E-cadherin defective” (n=12) or “E-cadherin wild-type” (n=22), and used these classifications to identify siRNAs that selectively targeted the E-cadherin defective cohort of breast tumour cell lines (Fig. 3A and B). We found that the “E-cadherin defective” or “E-cadherin wild-type” status defined by western blotting was

consistent with E-cadherin protein expression data determined by mass spectrometry (MS) (20), as well as E-cadherin mRNA expression and *CDH1* mutation data (Fig. 3C and D; Supplementary Table S5). For example, each of the tumour cell line models with *CDH1* truncating mutations or homozygous deletions lacked E-cadherin protein expression; similarly breast tumour cell lines with *CDH1* promoter hypermethylation (1,21), also lacked full length E-cadherin protein (Fig. 3A). Using the siRNA Achilles' Heel screen data (19) (Fig. 3B), we identified 31 siRNAs that selectively targeted the E-cadherin deficient cohort ($p < 0.05$, median permutation t-test), including ROS1 (Fig. 3E; Supplementary Fig. S4A and B median permutation t-test $p = 0.04$; Supplementary Table S6). We also assessed whether MET or ALK siRNA selectively targeted E-cadherin defective breast tumour cells, but in an analysis of 34 breast tumour cell lines, classified according to E-cadherin status (Supplementary Table S5), did not identify a significant association (Supplementary Fig. S5).

We also interrogated previously published siRNA Achilles' Heel screen data describing the kinase dependencies in an additional 69 non-breast cancer derived tumour cell lines (19). After annotating these according to E-cadherin status, we also noted a ROS1/E-cadherin synthetic lethal effect, suggesting that this effect was not necessarily specific to breast tumour models (Supplementary Fig. S6A-C; Supplementary Table S7). Validation experiments confirmed the ROS1/E-cadherin synthetic lethality in the breast tumour cell line models (Supplementary Fig. S7A-E), suggesting that this effect was not isolated to isogenic models, but also operated in molecularly diverse models of breast cancer.

We also used an orthogonal analytical approach, REVEALER (Repeated evaluation of variables conditional entropy and redundancy (22), to identify the molecular features found in breast tumour cell lines that were most associated with sensitivity to ROS1 siRNA. REVEALER uses a set of molecular features (e.g. the presence or

absence of mutations or other defects in key cancer driver genes or proteins) and target inhibition data (in this case sensitivity to ROS1 siRNA) from tumour cell line profiling experiments to identify multiple, often complimentary, molecular features that correlate with target inhibition, quantifying these effects as non-linear information correlation coefficients (ICs), between 1 (perfect correlation/features associated with resistance to target inhibition) and –1 (perfect negative correlation/features associated with sensitivity to target inhibition); REVEALER ICs <–0.1 or >0.1 are regarded as profound correlations (22). We carried out a REVEALER analysis using the ROS1 siRNA Z score data in the breast tumour cell lines as the measure of target inhibition and the mutational status of the 23 recurrently mutated cancer driver genes in the breast tumour cell line panel plus the E-cadherin protein classification described above as molecular features. Using this approach, we found E-cadherin protein deficiency to have a far greater correlation with ROS1 siRNA Z score (IC -0.5) than any of the other molecular features analysed (Fig. 3F), supporting the hypothesis that E-cadherin status is an important determinant of sensitivity to ROS1 inhibition in breast cancer. We also assessed the sensitivity of the breast tumour cell line panel to foretinib or crizotinib and found that the E-cadherin defective models were more sensitive to both inhibitors (Fig. 3G and H; Supplementary Table S8). The median sensitivity to either foretinib or crizotinib in the E-cadherin defective cohort was also similar to that in the *SLC34A2-ROS1* translocated HCC78 tumour cell line model (Fig. 3G and H). The responses to ROS1 inhibitors observed in the tumour cell line panel appeared to be independent of epithelial or mesenchymal status. For example, MCF10A cells do not undergo EMT upon loosing E-cadherin expression (23) but did exhibit both foretinib and crizotinib sensitivity (Fig. 2H-J). Similarly, SUM149, a mesenchymal breast tumour cell line which has wild type E-cadherin expression (24) was not sensitive to ROS1 inhibition, whereas E-cadherin defective, epithelial cells (e.g. SUM44, SKBR3) were (Supplementary Fig. S8). Furthermore, we did not find that expression of MET, ALK, pAKT, AKT, pERK or ERK correlated with

E-cadherin status, nor drug sensitivity (Supplementary Fig. S9), suggesting that these were unlikely to be determinants of the synthetic lethal effects we identified. As *ROS1* fusion genes are well established biomarkers of ROS1 inhibitor sensitivity we also analysed paired-end RNA-sequencing data using *Chimerascan* in order to identify ROS1 fusion genes in our tumour cell line panel (25,26). Whilst *Chimerascan* identified the *SLC34A2-ROS1* fusion event in HCC78 lung tumour cells (the positive control), *ROS1* fusions were not identified in any of the breast tumour cell lines (Supplementary Table S9). In addition, *ROS1* copy number or ROS1 variants, although rare in our tumour cell line panel, did not appear to correlate with crizotinib/foretinib sensitivity (Supplementary Table S9). We did note an increase in ROS1 expression and phospho-ROS1 levels in E-cadherin defective cells, similar to that seen in E-cadherin isogenic systems (Fig. 1F-H; Supplementary Fig. S10), suggesting that enhanced ROS1 expression could represent a homeostatic response to E-cadherin loss. Finally, we interrogated recently published data describing drug sensitivity effects in *ex vivo* cultured breast cancer explants (27) to identify drug sensitivity effects associated with loss of E-cadherin. When querying this data for drug sensitivity effects associated with *CDH1* gene copy number loss, we found sensitivity to crizotinib (PF-02341066 (27)) to be the most significant effect (Fig. 3I, *p* value 0.00127). The mean area under the curve (AUC) for crizotinib was 0.0713 in explants with *CDH1* copy number loss (n = 5) and 0.138 in explants without *CDH1* copy number loss (n = 12; False Discovery Rate (FDR) 0.214).

ROS1 inhibitors elicit synthetic lethality in endocrine resistant, E-cadherin defective, breast tumour cells and in models of E-cadherin defective gastric cancer

Given the central role of endocrine therapy in the treatment of ER+ve breast cancers and the frequency at which endocrine resistance develops, especially in the advanced disease setting (28), we assessed whether E-cadherin siRNA caused foretinib or crizotinib, sensitivity in previously-validated, endocrine therapy resistant, MCF7 LTED cells (29). We found that E-cadherin siRNA caused both foretinib and crizotinib sensitivity in MCF7 LTED cells ($p < 0.0001$, ANOVA, Fig. 4A-E) as it did in endocrine sensitive MCF7 cells (Fig. 2G), suggesting that the E-cadherin foretinib/crizotinib synthetic lethal effects were somewhat independent of endocrine therapy sensitivity. We also found that ER+ve, *de novo* endocrine resistant and E-cadherin defective MDAMB134VI tumour cells, which were derived from a case of invasive lobular carcinoma (30), were sensitive to ROS1 inhibitors in both *in vitro* (Supplementary Fig. S11A) and *in vivo* experiments (Supplementary Fig. S11B-D), suggesting that ROS1 inhibition could also target E-cadherin defective breast tumour cells in this particular setting.

We next assessed whether crizotinib or foretinib sensitivity extended to models of E-cadherin defective diffuse gastric cancer, given the elevated frequency of E-cadherin defects in this cancer subtype. We found that either crizotinib or foretinib selectively targeted E-cadherin defective gastric tumour cell lines (Supplementary Fig. S12A and B). The effects of crizotinib in additional gastric tumour cell lines have also been recently assessed (27,31). We reanalyzed this data and found that those tumour cells lines with reduced E-cadherin expression (defined by *CDH1* mRNA levels) were more sensitive to crizotinib than those with higher E-cadherin expression (Supplementary Fig. S12C).

ROS1 inhibition exacerbates p120 catenin, cleavage furrow and cytokinesis defects in E-cadherin defective cells

In investigating the cellular phenotypes associated with these E-cadherin selective effects, we found that exposure of E-cadherin defective cells to foretinib caused an increase in the proportion of cells with >4N DNA content (Fig. 5A and B), an increase in the frequency of cells with abnormal mitoses, particularly cells with multiple nuclei (Fig. 5C-F), an increase in expression of the G_2/M DNA damage biomarker p21 (Fig. 5G) and an increase in cellular apoptosis as assessed by PARP cleavage and caspase 3/7 activity (Fig. 5H-L; Supplementary Fig. S13). These phenotypes were reminiscent of those seen in Rhabdomyosarcoma tumour cells exposed to crizotinib (32) and Chronic Myeloid Leukemia (CML) tumour cell lines, where foretinib elicits phenotypes associated with mitotic catastrophe (MC) including multinucleated giant cells, increased DNA content and apoptotic cell death (33).

To assess what might cause such multinuclear phenotypes, we visualised cells exposed to crizotinib or foretinib using live cell microscopy. We found that in both E-cadherin wild type and defective cells, either foretinib or crizotinib extended the time cells spent in mitosis (Supplementary Fig. S14A and B). This extended mitosis had dichotomous effects, depending upon the status of E-cadherin. In E-cadherin wild type cells, exposure to a ROS1 inhibitor still resulted in the formation of two mononuclear daughter cells (Fig. 6A). In contrast, when exposed to a ROS1 inhibitor, E-cadherin defective cells initiated cytokinesis but failed to complete invagination of the cell membrane at the cleavage furrow, resulting in the formation of multinuclear cells (Fig. 6A). We noted that cytokinesis in E-cadherin defective cells exposed to foretinib or crizotinib was characterized by prolonged membrane oscillation, starting at the onset of anaphase, cleavage furrow regression resulting in multinucleated

cells, and also the formation of cells with lagging chromosomes (Fig. 6A; Supplementary Fig. S15; Supplementary Video S1-S5).

Cytokinesis failure and a multinuclear phenotype have previously been associated with defective p120-catenin activity (p120) (34,35). Actomyosin contractility at the ingression and cleavage furrow during anaphase and telophase is controlled by p120, which mediates these effects *via* binding to the centralspindlin component MKLP1 and the GTPase RhoA (35). p120 catenin also normally interacts with E-cadherin at the cell membrane where it is tyrosine phosphorylated (36-38), raising the possibility that loss of E-cadherin could impair p120 function. We found that E-cadherin defective tumour cells exhibited a reduction in p120–catenin levels (Fig. 6B), consistent with recent findings from a large-scale analysis of breast tumours with/without E-cadherin defects (39). Furthermore, as well as ROS1 immunoprecipitating with p120 (Fig. 6C), we found that ROS1 inhibition: (i) exacerbated the p120 reduction seen in E-cadherin defective cells; (ii) reduced tyrosine phosphorylation of p120; and (iii) reduced p120 levels at the cleavage furrow (Fig. 6B-C; Supplementary Fig. S16A and B). We also found that siRNA-mediated gene silencing of p120 (or ROS1) caused a multinuclear phenotype and elicited synthetic lethality in E-cadherin defective but not E-cadherin wild type cells (Fig. 6D-G). In normal epithelial cells, two opposing forces facilitate cytokinesis: (i) force provided by E-cadherin-dependent adherens junctions (AJ) at the apical membrane; and (ii) force provided by the contraction of the actomyosin ring at the cleavage furrow (40). One model to explain our observations might be that loss of one of these opposing forces in E-cadherin defective cells causes a greater reliance on processes and proteins that control cleavage furrow formation, such as p120 catenin. Our data suggest that ROS1 inhibitors exacerbate an existing p120 defect in E-cadherin defective cells and impair cytokinesis to such an extent that abnormal mitoses form; this elicits a DNA damage response (e.g. induction of p21

and γH2AX) and ultimately apoptosis. ROS1 inhibition has lesser effects when buffered by the activity of wild type E-cadherin.

Consistent with the concept that E-cadherin defects might cause a dependency upon processes controlled by actomyosin networks, such as cleavage furrow maturation, we also noted that the Rho GTPase effector kinase CDC42BPA (CDC42-binding kinase, MRCKα) which controls actomyosin function (41) was also identified as a robust synthetic lethal effect in our earlier siRNA screens (Supplementary Fig. S4A and B). We validated this synthetic lethal effect in subsequent experiments, including those using a toolbox small molecule MRCKα inhibitor (42) (Supplementary Fig. S17A-D), suggesting that additional targets associated with these processes might exist in E-cadherin defective cancers.

ROS1/E-cadherin synthetic lethality operates in multiple *in vivo* models of breast cancer

To assess the *in vivo* therapeutic potential of foretinib and crizotinib, we tested the ability of these drugs to affect the growth of E-cadherin defective invasive mammary carcinomas derived from the *K14cre;Cdh1$^{F/F}$;Trp53$^{F/F}$* (KEP) mouse ILC model; these mammary carcinomas show a strong resemblance to human ILC (43,44). E-cadherin defective mammary tumours from *K14cre;Cdh1$^{F/F}$;Trp53$^{F/F}$* (KEP) female mice were orthotopically transplanted into recipient mice and once established, animals were treated with foretinib, crizotinib or drug vehicle. In mice that received the drug vehicle alone, tumour growth continued unabated; in contrast, either foretinib or crizotinib treatment had a strong anti-tumour effect, reduced tumour volume and extended the survival of tumour-bearing mice (Fig. 7A-H, ANOVA $p < 0.0001$ in each case). Foretinib or crizotinib treatment also elicited a reduction in the proliferative index of tumours (as estimated by Ki67 immunohistochemistry) and an apoptotic response (Fig. 7D). The reduction in tumour volume in the early stages of crizotinib treatment is

highlighted in Fig. 7F. Similar studies in mice bearing MCF7^{A02} or MCF7^{Parental} derived xenografts also established that the anti-tumour effect of foretinib was significantly enhanced by the absence of E-cadherin (Supplementary Fig. S18A-E). We also assessed the anti-tumour effect of foretinib treatment in an E-cadherin defective patient-derived breast tumour xenograft (PDX) model, BCM2665, which was derived from a female with ER-negative, HER2-negative, basal-like breast cancer (Fig. 7I) (45). As before, foretinib significantly inhibited the growth of established tumours ($p < 0.0001$, ANOVA) and extended the survival of mice (Fig. 7J and K). E-cadherin defective tumours from mice treated with foretinib also consistently exhibited a profound reduction in levels of Ki67, suggesting a severe impairment in proliferative rate, showed increased levels of cleaved caspase-3, a marker of tumour cell apoptosis and had reduced hematoxylin and eosin staining, suggesting tumour necrosis (Fig. 7L). Given the availability of an immunohistochemical assay for measuring total and phosphorylated ROS1 in human tumours, we also established that foretinib treatment resulted in a decrease in pROS1 and total ROS1 (Supplementary Fig. S19).

Discussion

E-cadherin defects are a common characteristic of human tumours. Here we show that ROS1 inhibition constitutes an E-cadherin synthetic lethal interaction that can be elicited with clinical inhibitors such as crizotinib or foretinib. These effects appear to be robust in the face of considerable molecular heterogeneity that exist between different isogenic models, distinct tumour cell lines, *ex vivo* breast tumour explants and two different mouse models of E-cadherin defective breast cancer. The profound anti-tumour effects seen in mice with E-cadherin defective tumours suggests that the observed synthetic lethal effect might also have translational utility. Several distinct approaches can be used to assess the potential of ROS1 inhibitors in E-cadherin defective cancers. For example, clinical trials in advanced forms of ILC, where E-

cadherin defects are common, might seem appropriate. In such trials, absence of E-cadherin using immunohistochemical analysis could be used to pre-select appropriate patients for treatment. As crizotinib is already used in the treatment of non-small cell lung cancer, and has been the subject of prior clinical safety assessment, this drug seems a reasonable candidate for testing in such trials.

Mechanistically, our data suggests that loss of E-cadherin imparts upon cells a dependency upon ROS1 that is likely related to the ability to undergo cytokinesis. Our work suggests that p120 defects could play a role in these phenotypes, but it also seems possible that other proteins contribute to the synthetic lethal phenotype. For example, we also found that other proteins associated with actomyosin control such as MRCKα are also synthetic lethal with E-cadherin defects; these could conceivably play a part in the ROS1/E-cadherin synthetic lethal effect. Whilst drug-like inhibitors of Rho effector kinases such as MRCKα are still in development (46), licenced drugs such as crizotinib, might provide an actionable approach to targeting E-cadherin defective cancers. Similarly, although we were able to elicit E-cadherin synthetic lethal effects with multiple different ROS1 siRNA reagents and to partially reverse crizotinib sensitivity with a p.G2032R mutant ROS1 fusion cDNA (Fig. 2), the anti-tumour therapeutic effect of drugs such as crizotinib or foretinib could also be influenced by inhibition of kinases other than ROS1. Although we were unable to elicit synthetic lethality with siRNAs for MET, ALK, AXL and KDR in isogenic or non-isogenic systems (Supplementary Fig. S2 and S5), we cannot formally exclude the possibility that other kinase targets of foretinib or crizotinib also contribute to the E-cadherin synthetic lethality. It seems possible that clinical studies where mechanisms of resistance to crizotinib in E-cadherin defective tumours are assessed will inform this area.

Materials and Methods

Materials and cell lines

Small-molecule inhibitors were obtained from SelleckChem. siRNAs were obtained from GE Dharmacon. Cell lines were obtained from American Type Culture Collection (ATCC) and European Collection of Cell Cultures (ECACC) in 2010-2011 and maintained according to the supplier's instructions as described in (19,47). The MCF10A CDH1$^{-/-}$ and MCF10A CDH1$^{+/+}$ isogenic cell lines, were obtained in 2014 from Sigma Aldrich, and maintained according to the supplier's instructions. At sixth-monthly intervals and prior to storage, the identity of each cell line was confirmed by short tandem repeat (STR) profiling of 10 loci using the GenePrint 10 system (Promega). At monthly intervals, mycoplasma testing of cell cultures was carried out using MycoAlert Mycoplasma Detection Kit (Lonza).

CRISPR-Cas9 targeting

MCF7 cells were targeted using the Edit-R-CRISPR-CAS9-gene engineering kit (GE Dharmacon) according to the supplier's instructions. The following crRNA sequence was used: 5'GCUGAGGAUGGUGUAAGCGAGUUUUAGAGCUAUGCUGUUUUG 3'. MCF7 cells were transfected in 24 well plates (100,000 cells/well) with tracerRNA, crRNA and Cas9 plasmid. 72 hours after transfection, cells were plated in 15 cm dishes and continuously cultured until colonies formed. Colonies were recovered and profiled using PCR and Sanger sequencing to determine the presence of *CDH1* mutations.

RNAi and small-molecule synthetic lethal screens

siRNA screens and small-molecule screens were performed as described in (19,48). See also Supplementary Materials and Methods for details.

Cell survival and apoptosis assays

Cell survival analysis was conducted as previously describes (49). See also Supplementary Materials and Methods for details.

Protein analysis

Whole-cell protein extracts were prepared from cells lysed in NP250 buffer (20 mM Tris pH 7.6, 1 mM EDTA, 0.5 % NP40, 250 mM NaCl); supplemented with protease inhibitor cocktail tablets (Roche, Burgess Hill, UK). Protein concentrations were measured using BioRad Protein Assay Reagent (BioRad, Hemel Hempstead, UK). For Western blot analysis, 50 μg of whole cell lysates were electrophoresed on Novex 4–12% gradient bistris pre-cast gels (Invitrogen) and immunoblotted overnight at 4°C with antibodies listed in Supplementary Table S11.

Confocal microscopy

Cells were plated on coverslips and exposed to drugs the following day. After drug exposure, cells were fixed in 4% (v/v) paraformaldehyde for 10 minutes, washed, permeabilized in 0.2% (v/v) Triton X-100 in PBS for 20 minutes, washed, and blocked in IFF (1% (w/v) bovine serum albumin, 2% (v/v) FBS in PBS) then immunostained with primary antibodies targeting F-Actin conjugated to Alexa Fluor 488 and Tubulin (Santa Cruz Biotech) and detected with a Texas red conjugated secondary antibody (Supplementary Table S11). DAPI staining was used to detect nuclei. Mitotic and nuclear phenotypes of at least 200 cells per condition were scored in each replicate experiment. Confocal experiments were imaged using Zeiss CLM700.

Time lapse microscopy

Time-lapse microscopy was performed in 6 well plates using a Diaphot inverted microscope (Nikon), in a humidified CO_2 chamber at 37°C, using a motorized stage

(Prior Scientific), controlled by Simple PCI software (Compix). Cells were first transfected with a mCherry-H2B plasmid, FACS sorted for mCherry-H2B to facilitate DNA visualization, and then exposed to foretinib or crizotinib for a 24 hour period, over which they were microscopically imaged. Sorting of cells is described in Supplementary Materials and Methods.

Cell cycle analysis

Measurements took place on a BD LSR II SORP flow cytometer (BD Biosciences, USA) equipped with a 488 nm blue laser, a 561 nm yellow laser, a 633 nm red laser and a 404 nm violet laser. Propidium Iodide was measured with 600 LP 610/20 BP. Cell population was gated in a FSC/SSC dot plot and doublets were gated out based on a DNA dye area/width dot plot. This cell population was further analyzed regarding its cell distribution (G1, S and G_2/M phase) using Flow Jo V software.

***In vivo* assessment of foretinib and crizotinib efficacy**

In vivo efficacy studies were conducted using *K14cre;Cdh1*$^{F/F}$*;Trp53*$^{F/F}$ (KEP) or BCM2665 PDX tumour bearing mice as previously described (45,50). Experiments on *K14cre;Cdh1*$^{F/F}$*;Trp53*$^{F/F}$ (KEP) tumour bearing mice were carried out at the Netherlands Cancer Institute according to local and international regulations and ethical guidelines, and were approved by the local animal experimental committee at the Netherlands Cancer Institute (DEC-NKI AvD:30100 2015 407 appendix 1, WP 5791 and WP 5900). Balb/c nudes were implanted with *K14cre;Cdh1*$^{F/F}$*;Trp53*$^{F/F}$ (KEP) tumour sections in their 4th mammary gland on the right side as described previously (50). Once tumours reached 200 mm^3 in volume, mice were randomized into cohorts who received either crizotinib/foretinib 25mg/kg or 50mg/kg a day via oral gavage for 28 days or the drug vehicle. Operators were blinded to which cohort received foretinib or crizotinib and which received vehicle. A surrogate of animal survival was used and defined by the amount of time taken for tumours to reach a

pre-agreed volume of 1500mm^3, at which point mice were sacrificed. Experiments using the BCM 2665 PDX model were conducted at the ICR according to local (UK Home Office) and international regulations and ethical guidelines, and were approved by the local animal experimental committee at the Institute of Cancer Research. Viably frozen fragments of the BCM2665 model (45) were obtained from Dr. Michael Lewis, Baylor College of Medicine, USA, under material transfer agreement and propagated in SCID-Beige and NSG hosts. SCID-beige host mice were obtained from Charles River at 21-28 day of age and were implanted with BCM2665 tumour fragments (~2mm in length) subcutaneously into the inguinal mammary fat pad following standard procedures. Once tumours measured 2 mm in diameter (assessed by palpation and caliper measurement), mice were randomized into cohorts who received either foretinib (25mg/kg) or the drug vehicle (1% hydroxypropylmethylcellulose, 0.2% SDS in H_2O) every other day (4 days per week) by oral gavage. Operators were blinded to which cohort received foretinib and which received vehicle. Tumour growth was monitored over time (assessed by palpation and caliper measurement) and a surrogate of animal survival defined by the amount of time taken for tumours to reach a pre-agreed 12mm diameter, at which point mice were sacrificed and tumours excised. Tumour volume was calculated using the formula: $V= (\pi \times \text{length} \times \text{width}^2/6)$, where the length is the largest tumour diameter and width is the perpendicular diameter. Statistical analysis was performed using Prism. Tumours were formalin-fixed paraffin-embedded and slides were stained with H&E, or immunohistochemistry with antibodies against Ki-67 and cleaved caspase-3 was undertaken using standard procedures.

Disclosure of Potential Conflicts of Interest

We have no conflicts of interest to declare.

Authors' Contributions

Conception and design: Ilirjana Bajrami, Alan Ashworth, Christopher J. Lord

Development of methodology: Ilirjana Bajrami, Rebecca Marlow, Marieke van de Ven, Rachel Brough, Helen N. Pemberton, Jessica Frankum, Fei Fei Song, Rumana Rafiq, Asha Konde, Malini Menon, James Campbell, Aditi Gulati, Rahul Kumar, Dragomir B. Krastev, Colm Ryan, Patrick W. Derksen, Jos Jonkers, Andrew N.J. Tutt, Alan Ashworth, Christopher J. Lord

Acquisition of data (provided animals, provided facilities, etc.): Ilirjana Bajrami, Rebecca Marlow, Marieke van de Ven, Rachel Brough, Helen N. Pemberton, Jessica Frankum, Fei Fei Song, Rumana Rafiq, Asha Konde, Malini Menon, James Campbell, Aditi Gulati, Rahul Kumar, Stephen J. Pettitt, Mark D. Gurden, Marta Llorca Cardenosa, Irene Chong, Lesley-Ann Martin, Mitch Dowsett, Patrycja Gazinska, Fredrik Wallberg, Spiros Linardopoulos, Colm Ryan, Patrick W. Derksen, Jos Jonkers, Andrew N.J. Tutt, Alan Ashworth, Christopher J. Lord

Analysis and interpretation of data (e.g., statistical analysis, biostatistics, computational analysis): Ilirjana Bajrami, Rebecca Marlow, Marieke van de Ven, James Campbell, Aditi Gulati, Rahul Kumar, Rachael Natrajan, Colm Ryan, Christopher J. Lord

Writing, review, and/or revision of the manuscript: All authors

Administrative, technical, or material support (i.e., reporting or organizing data, constructing databases): Ilirjana Bajrami, Rachel Brough, Helen N. Pemberton, Jessica Frankum, Fei Fei Song, Rumana Rafiq, Asha Konde, Malini Menon, James Campbell, Aditi Gulati, Rahul Kumar, Stephen J. Pettitt, Elinor J. Sawyer, Christopher J. Lord

Study supervision: Alan Ashworth, Christopher J. Lord

Grant Support

This study was funded by Programme Grant funding to CJL from Breast Cancer Now (CTR-Q4-Y2) as part of funding to the Breast Cancer Now Toby Robins Research Centre and Programme Grant funding to CJL from CRUK (C30061/A24439). PWBD is supported by a grant from the Royal Dutch Cancer Society (KWF UU 2011-5203). MJLC is funded by a pre-doctoral grant from the Carlos III Health Institute (PFIS16/000246) and CIBERONC, an initiative of the Carlos III Health Institute (CB16/12-00473). CJR is a Sir Henry Wellcome Fellow jointly funded by Science Foundation Ireland, the Health Research Board, and the Wellcome Trust (103049/Z/13/Z) under the SFI-HRB-Wellcome Trust Biomedical Research Partnership.

Acknowledgments

We thank the late Chris Marshall FRS and members of his laboratory at The Institute of Cancer Research, London for helpful discussions. We thank members of the Breast Cancer Now Toby Robins Breast Cancer Research Centre Core Pathology Laboratory for pathology support. We also thank members of the Preclinical Intervention Unit of the Mouse Clinic for Cancer and Ageing (MCCA) at the Netherlands Cancer Institute and members of the Biological Services Unit at the ICR for *in vivo* study support. This work was funded by Breast Cancer Now as part of

programme funding to CJL. We acknowledge NHS funding to the NIHR Royal Marsden Hospital Biomedical Research Centre.

References

1. Ciriello G, Gatza ML, Beck AH, Wilkerson MD, Rhie SK, Pastore A*, et al.* Comprehensive Molecular Portraits of Invasive Lobular Breast Cancer. *Cell* **2015**;163:506-19.
2. Jeanes A, Gottardi CJ, Yap AS. Cadherins and cancer: how does cadherin dysfunction promote tumor progression? *Oncogene* **2008**;27:6920-9.
3. Lecuit T, Yap AS. E-cadherin junctions as active mechanical integrators in tissue dynamics. *Nat Cell Biol* **2015**;17:533-9.
4. Christgen M, Derksen P. Lobular breast cancer: molecular basis, mouse and cellular models. *Breast Cancer Res* **2015**;17:16.
5. Desmedt C, Zoppoli G, Gundem G, Pruneri G, Larsimont D, Fornili M*, et al.* Genomic Characterization of Primary Invasive Lobular Breast Cancer. *J Clin Oncol* **2016**;34:1872-81.
6. Michaut M, Chin SF, Majewski I, Severson TM, Bismeijer T, de Koning L*, et al.* Integration of genomic, transcriptomic and proteomic data identifies two biologically distinct subtypes of invasive lobular breast cancer. *Sci Rep* **2016**;6:18517.
7. Sikora MJ, Jankowitz RC, Dabbs DJ, Oesterreich S. Invasive lobular carcinoma of the breast: patient response to systemic endocrine therapy and hormone response in model systems. *Steroids* **2013**;78:568-75.
8. Metzger Filho O, Giobbie-Hurder A, Mallon E, Gusterson B, Viale G, Winer EP*, et al.* Relative Effectiveness of Letrozole Compared With Tamoxifen for Patients With Lobular Carcinoma in the BIG 1-98 Trial. *J Clin Oncol* **2015**;33:2772-9.
9. Knauer M GC, Dietze O, Greil R, Stöger H, Rudas M, Bago-Horvath Z, Mlineritsch B, Kwasny W, Singer C, Dubsky P, Jakesz R, Fitzal F, Steger G, Bartsch R, Filipits M, Fesl C, Gnant M. Survival advantage of anastrozol compared to tamoxifen for lobular breast cancer in the ABCSG-8 study. *Cancer Res* **2015**;75:nr S2-06.
10. Christgen M, Steinemann D, Kuhnle E, Langer F, Gluz O, Harbeck N*, et al.* Lobular breast cancer: Clinical, molecular and morphological characteristics. *Pathol Res Pract* **2016**;212:583-97.
11. Cristofanilli M, Gonzalez-Angulo A, Sneige N, Kau SW, Broglio K, Theriault RL*, et al.* Invasive lobular carcinoma classic type: response to primary chemotherapy and survival outcomes. *J Clin Oncol* **2005**;23:41-8.
12. Kashiwagi S, Yashiro M, Takashima T, Nomura S, Noda S, Kawajiri H*, et al.* Significance of E-cadherin expression in triple-negative breast cancer. *Br J Cancer* **2010**;103:249-55.
13. Shen T, Zhang K, Siegal GP, Wei S. Prognostic Value of E-Cadherin and beta-Catenin in Triple-Negative Breast Cancer. *Am J Clin Pathol* **2016**;146:603-10.
14. Ashworth A, Lord CJ, Reis-Filho JS. Genetic interactions in cancer progression and treatment. *Cell* **2011**;145:30-8.
15. Davare MA, Saborowski A, Eide CA, Tognon C, Smith RL, Elferich J*, et al.* Foretinib is a potent inhibitor of oncogenic ROS1 fusion proteins. *Proc Natl Acad Sci U S A* **2013**;110:19519-24.
16. Kuleshov MV, Jones MR, Rouillard AD, Fernandez NF, Duan Q, Wang Z*, et al.* Enrichr: a comprehensive gene set enrichment analysis web server 2016 update. *Nucleic Acids Res* **2016**;44:W90-7.
17. Zou HY, Li Q, Engstrom LD, West M, Appleman V, Wong KA*, et al.* PF-06463922 is a potent and selective next-generation ROS1/ALK inhibitor capable of blocking crizotinib-resistant ROS1 mutations. *Proc Natl Acad Sci U S A* **2015**;112:3493-8.

18. Awad MM, Katayama R, McTigue M, Liu W, Deng YL, Brooun A*, et al.* Acquired resistance to crizotinib from a mutation in CD74-ROS1. *N Engl J Med* **2013**;368:2395-401.
19. Campbell J, Ryan CJ, Brough R, Bajrami I, Pemberton HN, Chong IY*, et al.* Large-Scale Profiling of Kinase Dependencies in Cancer Cell Lines. *Cell Rep* **2016**;14:2490-501.
20. Lawrence RT, Perez EM, Hernandez D, Miller CP, Haas KM, Irie HY*, et al.* The proteomic landscape of triple-negative breast cancer. *Cell Rep* **2015**;11:630-44.
21. Hollestelle A, Nagel JH, Smid M, Lam S, Elstrodt F, Wasielewski M*, et al.* Distinct gene mutation profiles among luminal-type and basal-type breast cancer cell lines. *Breast Cancer Res Treat* **2010**;121:53-64.
22. Kim JW, Botvinnik OB, Abudayyeh O, Birger C, Rosenbluh J, Shrestha Y*, et al.* Characterizing genomic alterations in cancer by complementary functional associations. *Nat Biotechnol* **2016**;34:539-46.
23. Chen A, Beetham H, Black MA, Priya R, Telford BJ, Guest J*, et al.* E-cadherin loss alters cytoskeletal organization and adhesion in non-malignant breast cells but is insufficient to induce an epithelial-mesenchymal transition. *BMC Cancer* **2014**;14:552.
24. Hollestelle A, Peeters JK, Smid M, Timmermans M, Verhoog LC, Westenend PJ*, et al.* Loss of E-cadherin is not a necessity for epithelial to mesenchymal transition in human breast cancer. *Breast Cancer Res Treat* **2013**;138:47-57.
25. Iyer MK, Chinnaiyan AM, Maher CA. ChimeraScan: a tool for identifying chimeric transcription in sequencing data. *Bioinformatics* **2011**;27:2903-4.
26. Klijn C, Durinck S, Stawiski EW, Haverty PM, Jiang Z, Liu H*, et al.* A comprehensive transcriptional portrait of human cancer cell lines. *Nat Biotechnol* **2015**;33:306-12.
27. Bruna A, Rueda OM, Greenwood W, Batra AS, Callari M, Batra RN*, et al.* A Biobank of Breast Cancer Explants with Preserved Intra-tumor Heterogeneity to Screen Anticancer Compounds. *Cell* **2016**;167:260-74 e22.
28. Johnston SR, Leary A, Martin LA, Smith IE, Dowsett M. Enhancing endocrine response with novel targeted therapies: why have the clinical trials to date failed to deliver on the preclinical promise? *Cancer* **2008**;112:710-7.
29. Chan CM, Martin LA, Johnston SR, Ali S, Dowsett M. Molecular changes associated with the acquisition of oestrogen hypersensitivity in MCF-7 breast cancer cells on long-term oestrogen deprivation. *J Steroid Biochem Mol Biol* **2002**;81:333-41.
30. Sikora MJ, Cooper KL, Bahreini A, Luthra S, Wang G, Chandran UR*, et al.* Invasive lobular carcinoma cell lines are characterized by unique estrogen-mediated gene expression patterns and altered tamoxifen response. *Cancer Res* **2014**;74:1463-74.
31. Liu YJ, Shen D, Yin X, Gavine P, Zhang T, Su X*, et al.* HER2, MET and FGFR2 oncogenic driver alterations define distinct molecular segments for targeted therapies in gastric carcinoma. *Br J Cancer* **2014**;110:1169-78.
32. Megiorni F, McDowell HP, Camero S, Mannarino O, Ceccarelli S, Paiano M*, et al.* Crizotinib-induced antitumour activity in human alveolar rhabdomyosarcoma cells is not solely dependent on ALK and MET inhibition. *J Exp Clin Cancer Res* **2015**;34:112.
33. Dufies M, Jacquel A, Robert G, Cluzeau T, Puissant A, Fenouille N*, et al.* Mechanism of action of the multikinase inhibitor Foretinib. *Cell Cycle* **2011**;10:4138-48.
34. Perez-Moreno M, Song W, Pasolli HA, Williams SE, Fuchs E. Loss of p120 catenin and links to mitotic alterations, inflammation, and skin cancer. *Proc Natl Acad Sci U S A* **2008**;105:15399-404.

35. van de Ven RA, de Groot JS, Park D, van Domselaar R, de Jong D, Szuhai K*, et al.* p120-catenin prevents multinucleation through control of MKLP1-dependent RhoA activity during cytokinesis. *Nat Commun* **2016**;7:13874.
36. Fukumoto Y, Shintani Y, Reynolds AB, Johnson KR, Wheelock MJ. The regulatory or phosphorylation domain of p120 catenin controls E-cadherin dynamics at the plasma membrane. *Exp Cell Res* **2008**;314:52-67.
37. Roura S, Miravet S, Piedra J, Garcia de Herreros A, Dunach M. Regulation of E-cadherin/Catenin association by tyrosine phosphorylation. *J Biol Chem* **1999**;274:36734-40.
38. Ozawa M, Ohkubo T. Tyrosine phosphorylation of p120(ctn) in v-Src transfected L cells depends on its association with E-cadherin and reduces adhesion activity. *J Cell Sci* **2001**;114:503-12.
39. Ryan CJ, Kennedy S, Bajrami I, Matallanas D, Lord CJ. A Compendium of Co-regulated Protein Complexes in Breast Cancer Reveals Collateral Loss Events. *Cell Syst* **2017**;5:399-409 e5.
40. Guillot C, Lecuit T. Adhesion disengagement uncouples intrinsic and extrinsic forces to drive cytokinesis in epithelial tissues. *Developmental cell* **2013**;24:227-41.
41. Zhao Z, Manser E. Myotonic dystrophy kinase-related Cdc42-binding kinases (MRCK), the ROCK-like effectors of Cdc42 and Rac1. *Small GTPases* **2015**;6:81-8.
42. Tan I, Lai J, Yong J, Li SF, Leung T. Chelerythrine perturbs lamellar actomyosin filaments by selective inhibition of myotonic dystrophy kinase-related Cdc42-binding kinase. *FEBS Lett* **2011**;585:1260-8.
43. Derksen PW, Braumuller TM, van der Burg E, Hornsveld M, Mesman E, Wesseling J*, et al.* Mammary-specific inactivation of E-cadherin and p53 impairs functional gland development and leads to pleomorphic invasive lobular carcinoma in mice. *Dis Model Mech* **2011**;4:347-58.
44. Derksen PW, Liu X, Saridin F, van der Gulden H, Zevenhoven J, Evers B*, et al.* Somatic inactivation of E-cadherin and p53 in mice leads to metastatic lobular mammary carcinoma through induction of anoikis resistance and angiogenesis. *Cancer Cell* **2006**;10:437-49.
45. Zhang X, Claerhout S, Prat A, Dobrolecki LE, Petrovic I, Lai Q*, et al.* A renewable tissue resource of phenotypically stable, biologically and ethnically diverse, patient-derived human breast cancer xenograft models. *Cancer Res* **2013**;73:4885-97.
46. Unbekandt M, Croft DR, Crighton D, Mezna M, McArthur D, McConnell P*, et al.* A novel small-molecule MRCK inhibitor blocks cancer cell invasion. *Cell Commun Signal* **2014**;12:54.
47. Brough R, Frankum JR, Sims D, Mackay A, Mendes-Pereira AM, Bajrami I*, et al.* Functional viability profiles of breast cancer. *Cancer Discov* **2011**;1:260-73.
48. Miller RE, Brough R, Bajrami I, Williamson CT, McDade S, Campbell J*, et al.* Synthetic Lethal Targeting of ARID1A-Mutant Ovarian Clear Cell Tumors with Dasatinib. *Mol Cancer Ther* **2016**;15:1472-84.
49. Bajrami I, Kigozi A, Van Weverwijk A, Brough R, Frankum J, Lord CJ*, et al.* Synthetic lethality of PARP and NAMPT inhibition in triple-negative breast cancer cells. *EMBO Mol Med* **2012**;4:1087-96.
50. Rottenberg S, Nygren AO, Pajic M, van Leeuwen FW, van der Heijden I, van de Wetering K*, et al.* Selective induction of chemotherapy resistance of mammary tumors in a conditional mouse model for hereditary breast cancer. *Proc Natl Acad Sci U S A* **2007**;104:12117-22.
51. Barretina J, Caponigro G, Stransky N, Venkatesan K, Margolin AA, Kim S*, et al.* The Cancer Cell Line Encyclopedia enables predictive modelling of anticancer drug sensitivity. *Nature* **2012**;483:603-7.

Figure 1. ROS1 inhibition is synthetic lethal with E-cadherin defects in isogenic models. A, Wild-type E-cadherin protein is lost in the *CDH1* CRISPR-Cas9 mutagenised MCF7^{A02} clone. Western blot illustrating E-cadherin expression in parental MCF7 cells (MCF7^{parental}) and the MCF7^{A02} clone is shown. Upper band is a glycosylated isoform of E-cadherin, the lower band representing the non-glycosylated form. **B,** Confocal microscopy images of MCF7^{parental} and MCF7^{A02} cells, illustrating loss of E-cadherin expression (green) in MCF7^{A02} cells. Nuclei are imaged with DAPI (blue). **C,** Light microscopy images of MCF7^{parental} and MCF7^{A02} cells, illustrating reduction in cell-cell contact in MCF7^{A02} cells. **D,** Volcano plot illustrating AUC ratios (MCF7^{A02} E-cadherin defective/MCF7 E-cadherin wild type parental cells) of 80 small molecule inhibitors assessed in the high-throughput screen. AUC ratio <1 indicates candidate E-cadherin synthetic lethal effects. Blue dots represent ROS1 inhibitors. **E,** Volcano plot of data from the siRNA SMARTpool sensitivity screens in cell lines described in (B). Blue dot highlights ROS1 siRNA identified in the screen as selectively targeting E-cadherin defective cells. **F,** ROS1 expression is upregulated in E-cadherin defective cells. Western blot showing expression of ROS1, MET and ALK in MCF10A CDH1$^{+/+}$ and MCF10A CDH1$^{-/-}$ cells. ACTIN expression is used as loading control. **G**, Illustrative confocal microscopy images indicating an increase in ROS1 expression in E-cadherin defective MCF10A CDH1$^{-/-}$ cells compared to MCF10A CDH1$^{+/+}$ cells. ROS1 expression is shown in red, E-cadherin in green and DNA in blue. **H**, Ectopic expression of E-cadherin in MCF7^{A02} E-cadherin defective cells reduces ROS1 expression. Western blot illustrating ROS1 expression in E-cadherin defective MCF7^{A02} cells transfected with *FLAG epitope-CDH1* cDNA. ACTIN is used as loading control.

Figure 2. Validation of ROS1 synthetic lethality in E-cadherin defective isogenic models. A, Western blot illustrating ROS1 silencing caused by four different ROS1 siRNAs (1, 2, 3 and 4) compared to two different non-targeting siRNAs (siCONT1, siCONT2). Uncropped western blot images are shown in Supplementary Fig. S20. **B,** and **C,** Bar charts illustrating cell inhibition caused by ROS1 siRNAs in $MCF7^{parental}$ and $MCF7^{A02}$ cells (B) and MCF10A $CDH1^{+/+}$ and MCF10A $CDH1^{-/-}$ cells (C). NPI = normalized percentage inhibition (compared to siCONT (NPI=1) and siPLK1 (NPI=0)). Error bars represent standard error of the mean (SEM) from three independent experiments. **D,** Bar chart illustrating the effect of 1 μM foretinib or crizotinib in $MCF7^{parental}$ compared to two additional E-cadherin defective clones, $MCF7^{B04}$ and $MCF7^{B05}$. Error bars represent SEM from three independent experiments. **E,** Western blot illustrating E-cadherin expression in $MCF7^{A02}$ cell line model transfected with a *FLAG epitope-CDH1* cDNA expression construct. **F,** Surviving fraction data from $MCF7^{A02}$, $MCF7^{parental}$ and $MCF7^{A02\ +FLAG\text{-}CDH1}$ cell lines exposed to 1μM foretinib, crizotinib and TAE684. Cells were transfected with *FLAG epitope-CDH1* cDNA and clones selected in G418. Clones expressing FLAG epitope-E-cadherin were exposed to 1 μM foretinib, crizotinib or TAE684 for six continuous days, at which point cell viability was assessed. **p*<0.05 Student's t-test as shown. **G,** Dot chart illustrating cell survival effects of ROS1/MET/ALK inhibitors in $MCF7^{parental}$ and $MCF7^{A02}$ cells. SF_{50} = surviving fraction 50 (concentration required to cause 50 % reduction in survival). **H,** and **I,** Dose-response survival curves in MCF10A $CDH1^{+/+}$ and MCF10A $CDH1^{-/-}$ cells exposed to foretinib for six days (H) or two weeks (I). Error bars represent SEM from three independent experiments. In each case, ANOVA *p* value MCF10A $CDH1^{+/+}$ *vs*. MCF10A $CDH1^{-/-}$ cells < 0.0001. Dose-response in *SLC34A2-ROS1* translocation-positive HCC78 cells is shown as a positive control. **J,** Dose-response survival curves in MCF10A $CDH1^{+/+}$ and MCF10A $CDH1^{-/-}$ cells exposed to ROS1 kinase inhibitor PF-06463922 for six days. Error bars represent SEM from three independent experiments. **K,** Dose-response survival

curves in MCF7^{A02} cells transfected with different concentrations of ROS1 siRNA SMARTpool and subsequently exposed to foretinib for six days. Increasing concentration of ROS1 siRNA caused a dose-dependent reduction in foretinib SF_{50}. Error bars represent SEM from three independent experiments. **L,** Expression of a crizotinib-refractory p.G2032R mutant *ROS1* fusion cDNA (18) causes crizotinib resistance in E-cadherin defective MCF10A CDH1-/- cells. Cells were transfected with either a p.G2032R *CD74-ROS1* cDNA expression vector or a cDNA expression vector without a *CD74-ROS1* insert ("empty"). Twenty-four hours after transfection, cells were exposed to crizotinib for a subsequent six days, at which point cell viability was assessed. Data shows the median effects of three independent experiments. Error bars illustrate the SEM. ***$p < 0.001$ Student's t test as shown.

Figure 3. Synthetic lethality of ROS1 inhibition in E-cadherin deficient breast tumour cell lines. A, Western blot illustrating E-cadherin expression in 37 breast tumour cell lines (including MCF7 as positive control). Cell line names are colour-coded according to the presence of *CDH1* gene mutations, gene deletion events or *CDH1* promoter hypermethylation events. Uncropped western blot images are shown in Supplementary Fig. S20. **B,** Schematic illustrating breast tumour cell line cohort sizes used to interrogate siRNA sensitivity screens (19). **C,** Bar chart illustrating E-cadherin expression of a subset of the breast tumour cell lines shown in (A), determined by mass spectrometry, described in (20). Western blot classification of E-cadherin status from (A) is shown. **D,** Scatter plot illustrating *CDH1* mRNA expression levels in breast tumour cell lines from the CCLE dataset (51). **E,** Volcano plot of data from the siRNA SMARTpool sensitivity screens described in (B). Blue dot highlights ROS1 siRNA identified in the screen as selectively targeting E-cadherin defective cells. **F,** REVEALER analysis identifies E-cadherin status as an important determinant of ROS1 siRNA sensitivity. Heatmap illustrates the REVEALER output identifying complementary genomic alterations associated with ROS1 siRNA

sensitivity in the 34 breast tumour cell line panel described in (B). IC (information correlation coefficient) scores and nominal *p* values with respect to the target are shown on the right side of the heatmap. E-cadherin status demonstrated the most profound IC score -0.5 from 23 molecular features examined. **G,** and **H,** Box whisker plots illustrating foretinib (G) or crizotinib (H) sensitivity in 12 breast tumour cell lines, defined by $\log_2$ area under the curve (AUC) values. Individual AUC values are listed in Supplementary Table S8. Log_2 AUC values for *SLC34A2-ROS1* translocation-positive HCC78 cells are shown as a positive control. ** *p* value = 0.003, Student's t-test, * *p* value =0.035 Student's t-test. **I,** Volcano plot of drug sensitivity effects in *ex vivo* cultured breast cancer explants (27) annotated according to *CDH1* gene copy number. Red dot highlights crizotinib as selectively targeting explants with *CDH1* gene copy number loss. Median AUC in explants with *CDH1* copy number loss = 0.0713, median AUC in explants without *CDH1* copy number loss = 0.138, *p* value =0.00127. Y-axis shows adjusted *p*-value ($-\log_{10}$) from a t-test comparing AUC in *ex vivo* explant models with *CDH1* loss *vs.* models with no *CDH1* copy number change. X-axis shows the negative value of the t-statistic describing the difference in AUC means for *ex vivo* explant models with *CDH1* loss *vs.* models with no *CDH1* copy number change. Negative values suggest drug sensitivity in *ex vivo* explant models with *CDH1* loss *vs.* models with no *CDH1* copy number change.

Figure 4. E-cadherin/ROS1 synthetic lethality is independent of endocrine therapy resistance. A, Dose-response survival curves in MCF7 and MCF7 LTED cells exposed to fulvestrant for five days. Error bars represent SEM from three independent experiments. **B,** and **C,** Dose-response survival curves in MCF7 LTED cells transfected with two independent E-cadherin (*CDH1*) siRNA reagents; siRNA 1 (B) and siRNA 2 (C) and a non-targeting siRNA (siCONT1) for 48 hours and subsequently exposed to foretinib or fulvestrant for five days. Error bars represent SEM from three independent experiments. ANOVA *p* value MCF7 LTED transfected

with two independent E-cadherin siRNA reagents *vs*. MCF7 LTED transfected with siCONT1 cells $p < 0.0001$ for foretinib. No statistically significant difference was observed in the same cells exposed to fulvestrant. **D,** and **E,** Dose-response survival curves in cells as in (B) and (C) exposed to crizotinib or fulvestrant for five days. Error bars represent SEM from three independent experiments. ANOVA *p* value MCF7 LTED transfected with two independent E-cadherin siRNA reagents *vs*. MCF7 LTED transfected with siCONT1 cells $p < 0.0001$ for crizotinib. No statistically significant difference was observed in the same cells exposed to fulvestrant.

Figure 5. Cell cycle and mitotic defects in E-cadherin defective cells. A, FACS plots illustrating increase in DNA content in E-cadherin defective $MCF7^{A02}$ cells exposed to foretinib. **B,** Enlarged image from (A) indicating >4n fraction. The fraction of cells with >4n DNA content is shown. **C,** Box whisker plots indicating fraction of cells with abnormal mitoses (e.g. multinuclear defects) in cells exposed to foretinib. *** *p* value = 0.0001, ** *p* value = 0.0054, Student's t-test. Nuclear defects were visualized by confocal microscopy and a minimum of 200 cells were counted for each cell line. Data is representative of two independent experiments in each case. **D,** Illustrative confocal microscopy images indicating multinuclear phenotype in E-cadherin defective $MCF7^{A02}$ cells exposed to foretinib. **E,** Illustrative confocal microscopy images indicating multinuclear phenotype in E-cadherin defective SKBR3 and BT549 cells and E-cadherin wild-type T47D and SUM149 cells exposed to 1μM foretinib. **F,** Box whisker plots indicating fraction of cells with abnormal mitoses (e.g. multinuclear defects) in cells exposed to foretinib. * *p*-value =0.021, Student's t-test. Data is representative of two independent experiments in each case. **G,** Western blot illustrating increased p21 levels in the E-cadherin defective $MCF7^{A02}$ cells exposed to 1μM foretinib *vs*. $MCF7^{parental}$ cells. **H,** Bar chart illustrating increased caspase 3/7 activity in E-cadherin defective cells exposed to either crizotinib or foretinib. Median effects from three independent experiments are shown, with error bars representing

the SEM. **I,** Bar chart illustrating increased caspase 3/7 activity in E-cadherin defective cells transfected with a siRNA targeting ROS1. siPLK1 was used as a positive control. *p<0.05* between E-cadherin defective *vs.* wild-type groups, using the Student's t-test. Median effects from three independent experiments are shown, with error bars representing the SEM. Bar chart illustrating increased caspase 3/7 activity in E-cadherin defective $MCF7^{A02}$ **J** BT549 **K** and SKBR3 **L** cells exposed to either crizotinib or foretinib, compared to E-cadherin wild type $MCF7^{Parental}$ cells. * $p < 0.01$, ** $p < 0.001$ and *** $p < 0.0001$, E-cadherin defective *vs.* $MCF7^{Parental}$ cells, Student's t-test. Median effects from three independent experiments are shown, with error bars representing the SEM.

Figure 6. ROS1 inhibition exacerbates p120 catenin and cytokinesis defects in E-cadherin defective cells (previous page). A, Time lapse microscopy images illustrating cell division in $MCF7^{Parental}$ (top panel) and E-cadherin defective $MCF7^{A02}$ (bottom panel) cells exposed to foretinib, crizotinib or vehicle. $MCF7^{A02}$ and $MCF7^{Parental}$ cells were first transfected with a mCherry-H2B plasmid, FACS sorted for mCherry-H2B to facilitate DNA visualization, and then exposed to foretinib, crizotinib or vehicle for a 24-hour period. Initial formation of the cleavage furrow, followed by formation of a multinuclear cell is highlighted with white arrows. Scale bar, 10 μm. **B**, Loss of E-cadherin is associated with a reduction in p120 levels and ROS1 inhibition causes a reduction in p120 tyrosine phosphorylation. Western blot showing phospho-p120 (Tyr228) and total p120 catenin levels in MCF10A $CDH1^{+/+}$ and MCF10A $CDH1^{-/-}$ cells, exposed to a range of foretinib concentrations (vehicle, 0.03 μM, 0.1 μM, 0.3 μM or 1 μM) for 16 hours. **C**, ROS1 interacts with p120. Western blot illustrating co-immunoprecipitation of GFP-p120 and FLAG-ROS1 proteins in $MCF7^{A02}$ cells. **D,** Western blot illustrating p120 catenin silencing caused by two different p120 siRNAs (sip120_1 and _2) compared to a non-targeting siRNA (siCONT1). **E,** p120 or ROS1 siRNA causes mitotic defects in E-cadherin defective

cells. Bar chart indicating fraction of cells with abnormal mitoses in cells transfected with siRNAs targeting p120 or ROS1 siRNAs. *** *p* value < 0.0001, ** *p* value < 0.001, Student's t-test. A minimum of 100 cells were analyzed for each cell line. Data is representative of three replica experiments, error bars represent SEM. **F,** p120 gene silencing is synthetically lethal with E-cadherin deficiency. Bar chart illustrating cell inhibition caused by two different p120 siRNAs (1 and 2) in E-cadherin wild type $MCF7^{Parental}$ and E-cadherin defective $MCF7^{A02}$ cells. NPI = normalized percentage inhibition (compared to non-targeting siRNA, siCONT (NPI=1) and cytotoxic siRNA targeting PLK1 (NPI=0)). Error bars represent standard error of the mean (SEM) from three independent experiments. *** *p* value < 0.0001, Student's t-test. **G,** Representative images from a colony forming assay illustrating cell inhibition caused by two different p120 siRNAs (1 and 2) or ROS1 siRNA in E-cadherin wild type $MCF7^{Parental}$ and E-cadherin defective $MCF7^{A02}$ cells. A non-targeting siRNA, siCONT and siPLK1 are used as controls.

Figure 7. E-cadherin synthetic lethal effects operate *in vivo* in E-cadherin defective breast tumours. A, Therapeutic response to foretinib treatment in mice bearing E-cadherin deficient mammary tumours. Mammary tumour fragments from KEP mice were transplanted into 22 recipient mice; once tumours had established, animals were treated over a 27-day period with either drug vehicle or foretinib (25 or 50 mg/kg every other day, n=8 for vehicle-treated cohorts and n=7 for each drug treatment cohort). Tumour volumes after the initiation of treatment are shown. ANOVA p<0.0001 for both foretinib treatment regimes compared to vehicle-treated mice. **B,** Kaplan–Meier plot of data from (A) indicating anti-tumour efficacy of 25 mg/kg foretinib treatment. Mice were sacrificed once tumours reached a volume of 1500 mm^3. **C,** Kaplan–Meier plot of data from (A) for vehicle *vs.* foretinib 50 mg/kg cohort. **D,** Immunohistochemistry images of tumours extracted from animals from (A) at the end of foretinib treatment are shown. Representative images of H&E, Ki67 and

cleaved Caspase 3 are shown (magnification = 20x). Scale bar represents 250µm. **E**, Therapeutic response to crizotinib treatment in mice bearing KEP tumour allografts as in (A). ANOVA p<0.0001 for both crizotinib treatment regimes compared to vehicle-treated mice. **F,** Data from (E)**,** plotted to illustrate tumour volume reduction in both crizotinib treated cohorts. **G,** Kaplan–Meier plot of data from (E), indicating effect of 25 mg/kg crizotinib treatment. **H,** Kaplan–Meier plot of data from (E) for vehicle *vs.* crizotinib 50 mg/kg cohort. **I,** Immunohistochemistry images illustrating lack of E-cadherin expression in a patient-derived xenograft (PDX) model of breast cancer (BCM2665) compared to positive (HCC1954 breast tumour cells) and negative controls (MDAMB231 breast tumour cells). **J,** Therapeutic response to foretinib treatment in mice bearing BCM2665 PDX. BCM2665 was transplanted into 19 recipient mice; once tumours had established, animals were treated over a 47-day period with either drug vehicle (n=11), or foretinib (25 mg/kg every other day, n= 8) as shown. ANOVA = p<0.0001. **K,** Kaplan–Meier plot of data from (I). **L,** Representative images of FFPE tumours from animals in (I) stained with H&E, Ki67 and cleaved caspase 3 are shown (magnification = 20x). Scale bar represents 250µm.

Figure 1

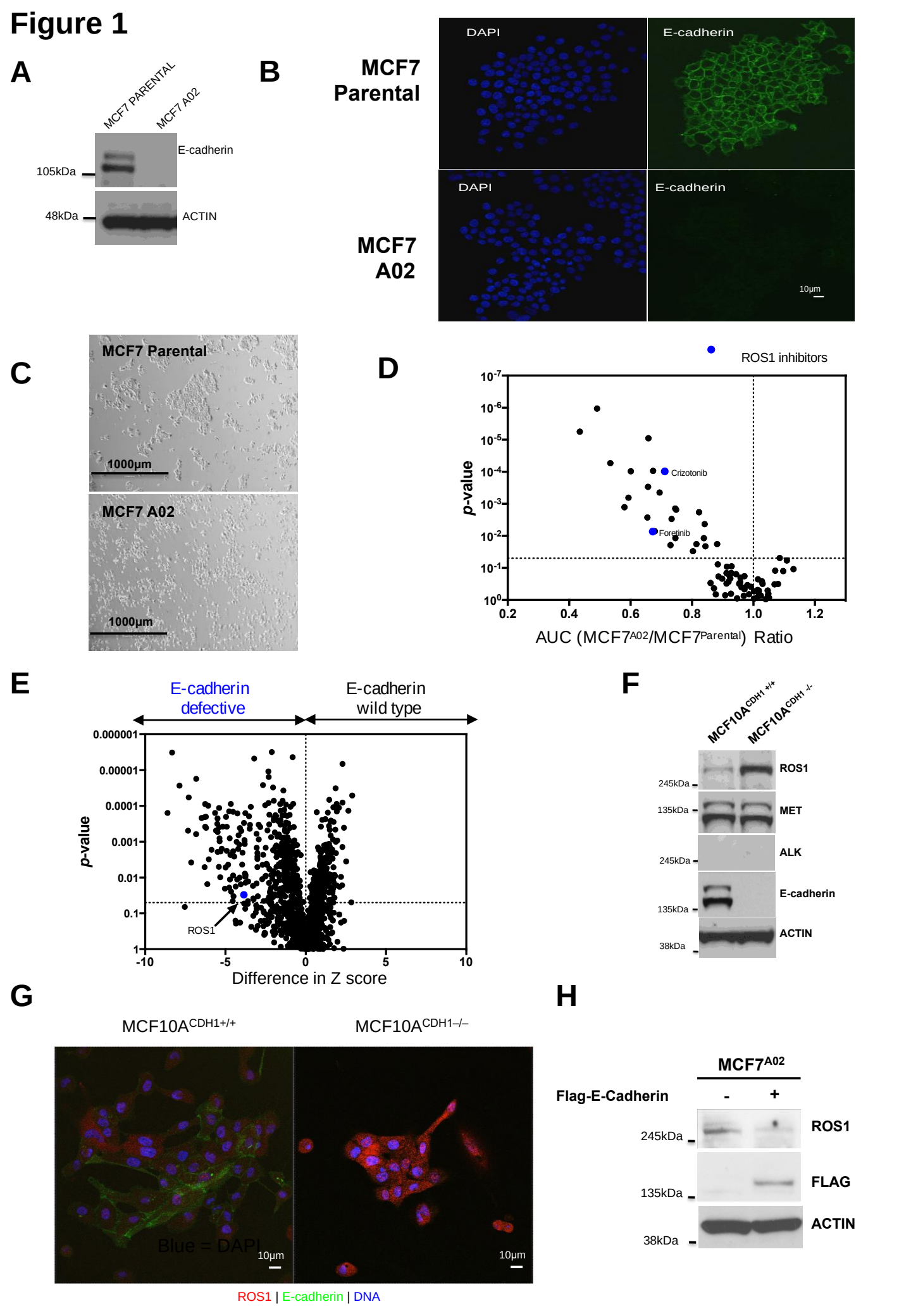
A
MCF7 PARENTAL
MCF7 A02
E-cadherin
105kDa
48kDa
ACTIN
B
MCF7 Parental
MCF7 A02
DAPI
E-cadherin
10μm
C
MCF7 Parental
1000μm
MCF7 A02
1000μm
D
ROS1 inhibitors
Crizotonib
Foretinib
p-value
AUC (MCF7A02/MCF7Parental) Ratio
E
E-cadherin defective
E-cadherin wild type
p-value
ROS1
Difference in Z score
F
MCF10ACDH1 +/+
MCF10ACDH1 -/-
ROS1
MET
ALK
E-cadherin
ACTIN
245kDa
135kDa
245kDa
135kDa
38kDa
G
MCF10ACDH1+/+
MCF10ACDH1–/–
Blue = DAPI
10μm
10μm
ROS1 | E-cadherin | DNA
H
MCF7A02
Flag-E-Cadherin
-
+
ROS1
FLAG
ACTIN
245kDa
135kDa
38kDa

Figure 2

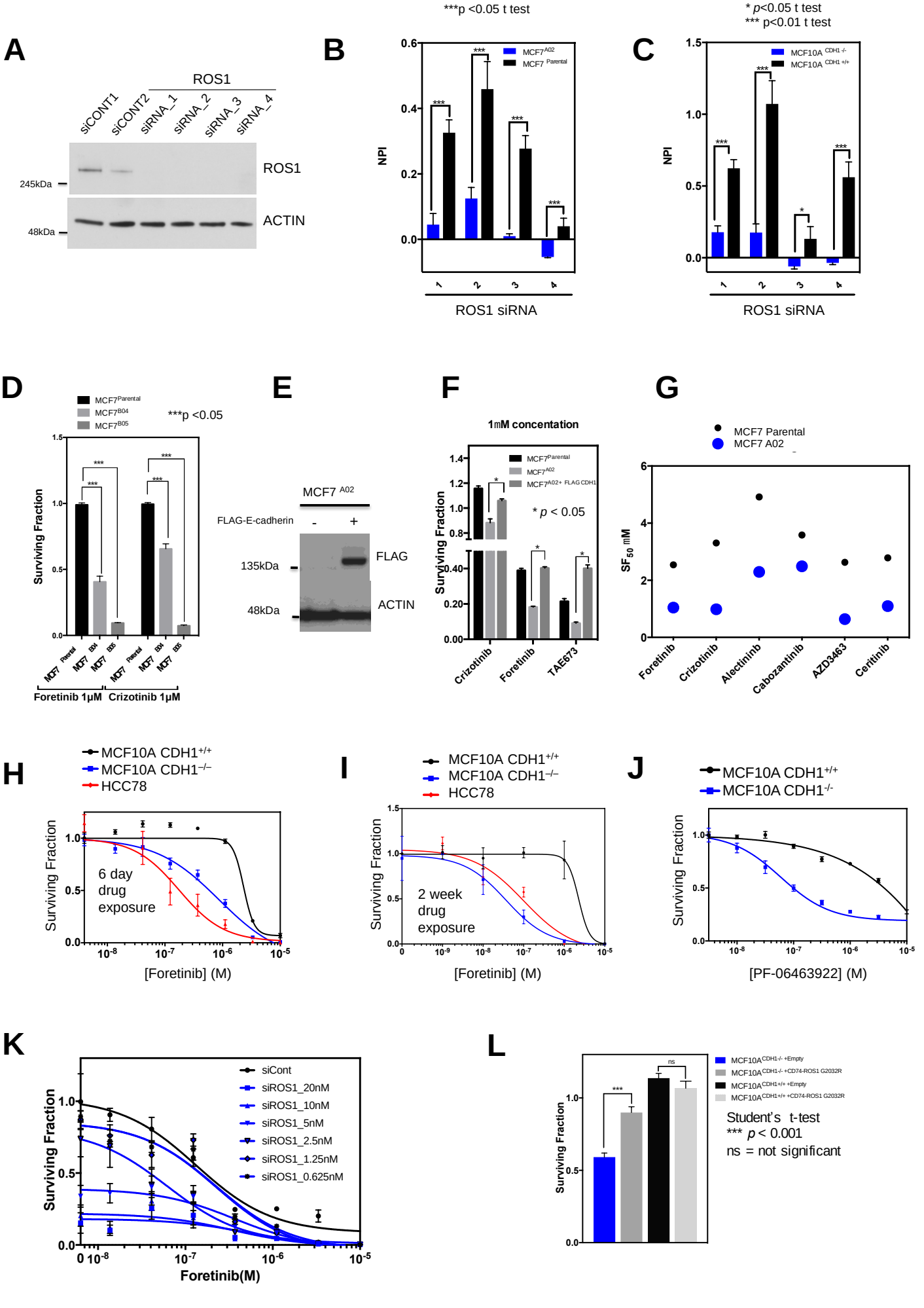
A
ROS1
siCONT1
siCONT2
siRNA_1
siRNA_2
siRNA_3
siRNA_4
245kDa
ROS1
48kDa
ACTIN
B
***p <0.05 t test
MCF7 A02
MCF7 Parental
NPI
ROS1 siRNA
C
* p<0.05 t test
*** p<0.01 t test
MCF10A CDH1 -/-
MCF10A CDH1 +/+
NPI
ROS1 siRNA
D
MCF7 Parental
MCF7 B04
MCF7 B05
***p <0.05
Surviving Fraction
Foretinib 1μM
Crizotinib 1μM
E
MCF7 A02
FLAG-E-cadherin
-
+
135kDa
FLAG
48kDa
ACTIN
F
1mM concentation
MCF7 Parental
MCF7 A02
MCF7 A02+ FLAG CDH1
* p < 0.05
Surviving Fraction
Crizotinib
Foretinib
TAE673
G
MCF7 Parental
MCF7 A02
SF50 nM
Foretinib
Crizotinib
Alectininb
Cabozantinib
AZD3463
Ceritinib
H
MCF10A CDH1+/+
MCF10A CDH1−/−
HCC78
Surviving Fraction
6 day drug exposure
[Foretinib] (M)
I
MCF10A CDH1+/+
MCF10A CDH1−/−
HCC78
Surviving Fraction
2 week drug exposure
[Foretinib] (M)
J
MCF10A CDH1+/+
MCF10A CDH1-/-
Surviving Fraction
[PF-06463922] (M)
K
siCont
siROS1_20nM
siROS1_10nM
siROS1_5nM
siROS1_2.5nM
siROS1_1.25nM
siROS1_0.625nM
Surviving Fraction
Foretinib(M)
L
ns
MCF10ACDH1-/- +Empty
MCF10ACDH1-/- +CD74-ROS1 G2032R
MCF10ACDH1+/+ +Empty
MCF10ACDH1+/+ +CD74-ROS1 G2032R
Surviving Fraction
Student's t-test
*** p < 0.001
ns = not significant

Figure 3

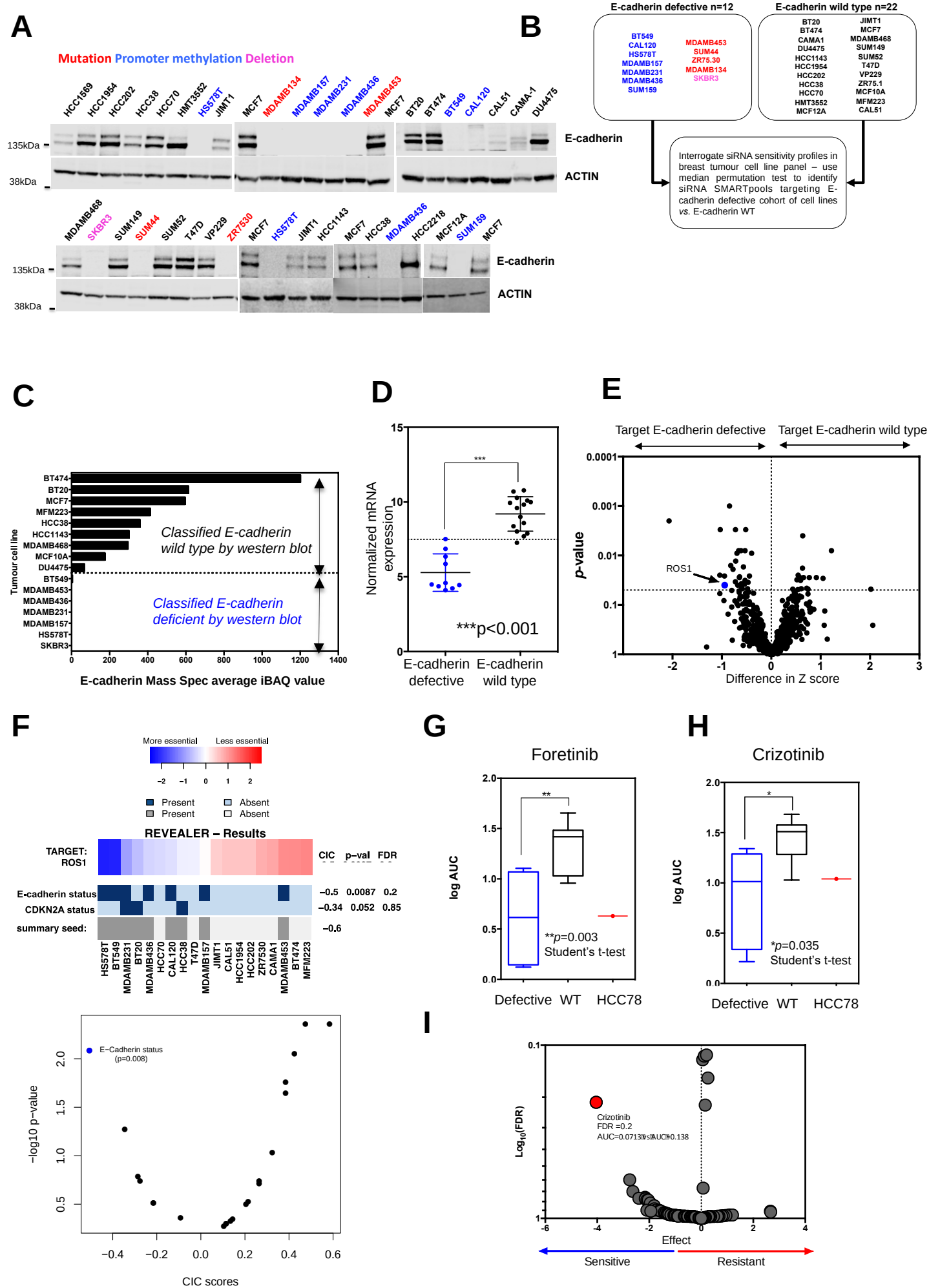
A
Mutation Promoter methylation Deletion
HCC1569 HCC1954 HCC202 HCC38 HCC70 HMT3552 HS578T JIMT1 MCF7 MDAMB134 MDAMB157 MDAMB231 MDAMB436 MDAMB453 MCF7 BT20 BT474 BT549 CAL120 CAL51 CAMA-1 DU4475
135kDa
38kDa
E-cadherin
ACTIN
MDAMB468 SKBR3 SUM149 SUM44 SUM52 T47D VP229 ZR7530 MCF7 HS578T JIMT1 HCC1143 MCF7 HCC38 MDAMB436 HCC2218 MCF12A SUM159 MCF7
135kDa
38kDa
E-cadherin
ACTIN
B
E-cadherin defective n=12
BT549 CAL120 HS578T MDAMB157 MDAMB231 MDAMB436 SUM159
MDAMB453 SUM44 ZR75.30 MDAMB134 SKBR3
E-cadherin wild type n=22
BT20 BT474 CAMA1 DU4475 HCC1143 HCC1954 HCC202 HCC38 HCC70 HMT3552 MCF12A
JIMT1 MCF7 MDAMB468 SUM149 SUM52 T47D VP229 ZR75.1 MCF10A MFM223 CAL51
Interrogate siRNA sensitivity profiles in breast tumour cell line panel – use median permutation test to identify siRNA SMARTpools targeting E-cadherin defective cohort of cell lines vs. E-cadherin WT
C
Tumour cell line
BT474 BT20 MCF7 MFM223 HCC38 HCC1143 MDAMB468 MCF10A DU4475 BT549 MDAMB453 MDAMB436 MDAMB231 MDAMB157 HS578T SKBR3
Classified E-cadherin wild type by western blot
Classified E-cadherin deficient by western blot
0 200 400 600 800 1000 1200 1400
E-cadherin Mass Spec average iBAQ value
D
Normalized mRNA expression
***
***p<0.001
E-cadherin defective
E-cadherin wild type
E
Target E-cadherin defective
Target E-cadherin wild type
p-value
ROS1
Difference in Z score
F
More essential
Less essential
Present
Absent
REVEALER – Results
TARGET: ROS1
CIC p-val FDR
E-cadherin status
CDKN2A status
summary seed:
−0.5 0.0087 0.2
−0.34 0.052 0.85
−0.6
HS578T BT549 MDAMB231 BT20 MDAMB436 HCC70 CAL120 HCC38 T47D MDAMB157 JIMT1 CAL51 HCC1954 HCC202 ZR7530 CAMA1 MDAMB453 BT474 MFM223
E−Cadherin status (p=0.008)
−log10 p−value
CIC scores
G
Foretinib
log AUC
**
**p=0.003
Student's t-test
Defective WT HCC78
H
Crizotinib
log AUC
*
*p=0.035
Student's t-test
Defective WT HCC78
I
Crizotinib
FDR =0.2
AUC=0.071 vs AUC=0.138
Log10(FDR)
Effect
Sensitive
Resistant

Figure 4

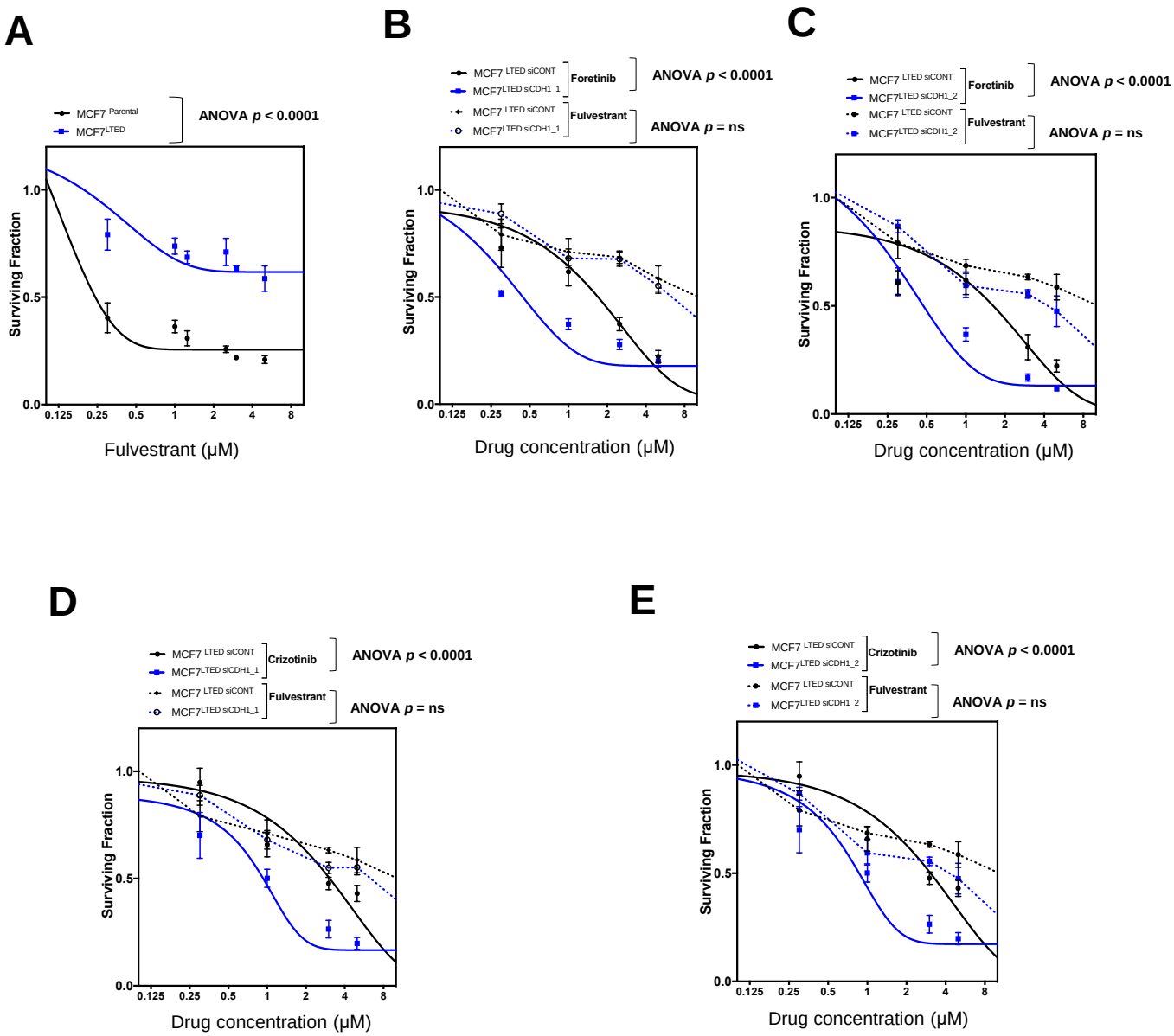
A
MCF7 Parental
MCF7LTED
ANOVA p < 0.0001
Surviving Fraction
Fulvestrant (μM)
B
MCF7 LTED siCONT
MCF7LTED siCDH1_1
Foretinib
ANOVA p < 0.0001
Fulvestrant
ANOVA p = ns
Drug concentration (μM)
C
MCF7 LTED siCONT
MCF7LTED siCDH1_2
Foretinib
ANOVA p < 0.0001
Fulvestrant
ANOVA p = ns
Drug concentration (μM)
D
Crizotinib
ANOVA p < 0.0001
Fulvestrant
ANOVA p = ns
Drug concentration (μM)
E
Crizotinib
ANOVA p < 0.0001
Fulvestrant
ANOVA p = ns
Drug concentration (μM)

Figure 5

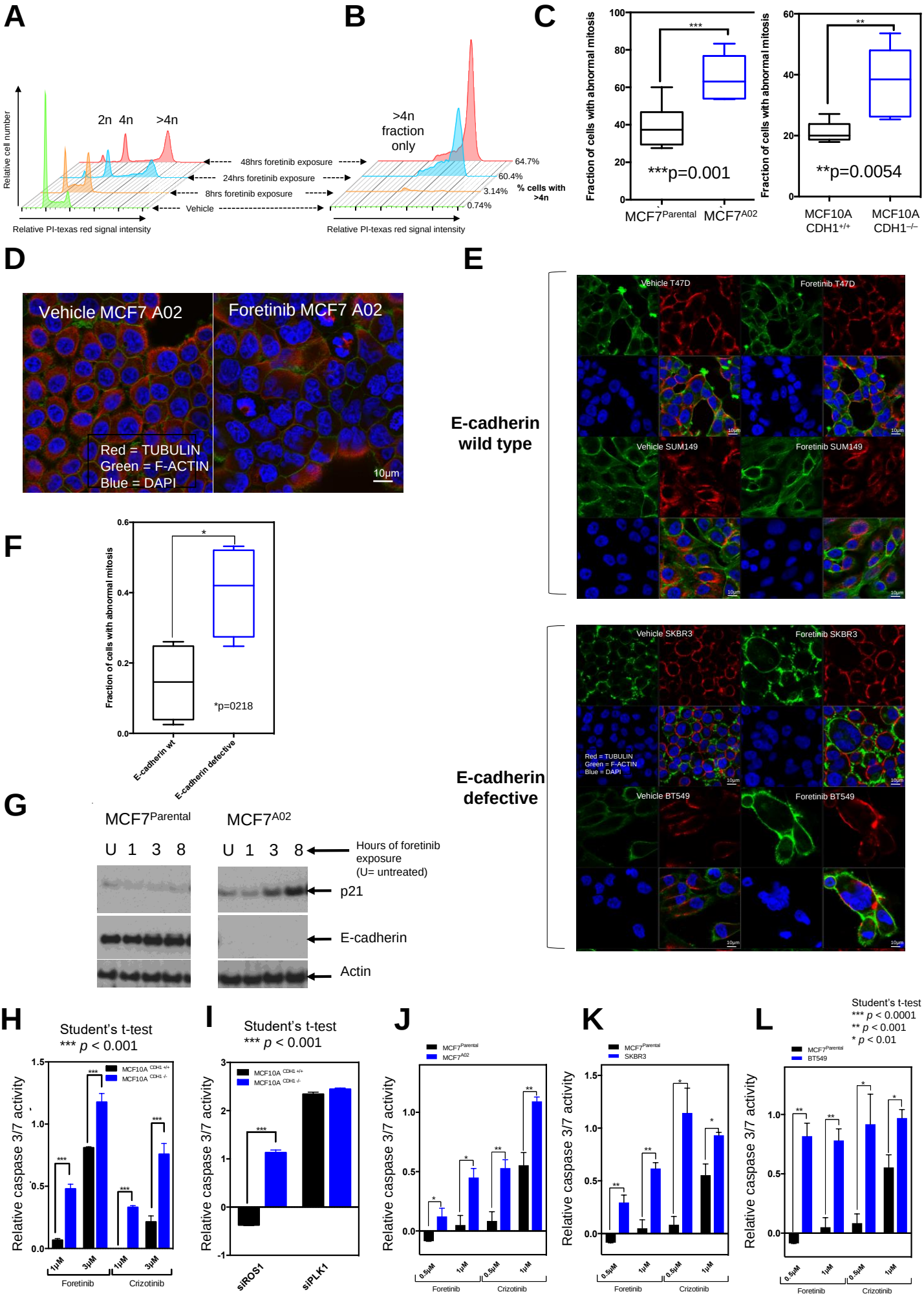
A
B
C
Relative cell number
2n 4n >4n
48hrs foretinib exposure
24hrs foretinib exposure
8hrs foretinib exposure
Vehicle
Relative PI-texas red signal intensity
>4n fraction only
64.7%
60.4%
3.14%
0.74%
% cells with >4n
Relative PI-texas red signal intensity
Fraction of cells with abnormal mitosis
***p=0.001
MCF7Parental
MCF7A02
**p=0.0054
MCF10A CDH1+/+
MCF10A CDH1−/−
D
Vehicle MCF7 A02
Foretinib MCF7 A02
Red = TUBULIN
Green = F-ACTIN
Blue = DAPI
10μm
E
E-cadherin wild type
Vehicle T47D
Foretinib T47D
Vehicle SUM149
Foretinib SUM149
E-cadherin defective
Vehicle SKBR3
Foretinib SKBR3
Vehicle BT549
Foretinib BT549
F
Fraction of cells with abnormal mitosis
*p=0218
E-cadherin wt
E-cadherin defective
G
MCF7Parental
MCF7A02
U 1 3 8
Hours of foretinib exposure (U= untreated)
p21
E-cadherin
Actin
H
Student's t-test
*** p < 0.001
Relative caspase 3/7 activity
MCF10A CDH1 +/+
MCF10A CDH1 -/-
1μM
3μM
Foretinib
Crizotinib
I
Student's t-test
*** p < 0.001
siROS1
siPLK1
J
MCF7Parental
MCF7A02
0.5μM
1μM
K
SKBR3
L
BT549
Student's t-test
*** p < 0.0001
** p < 0.001
* p < 0.01

Figure 6

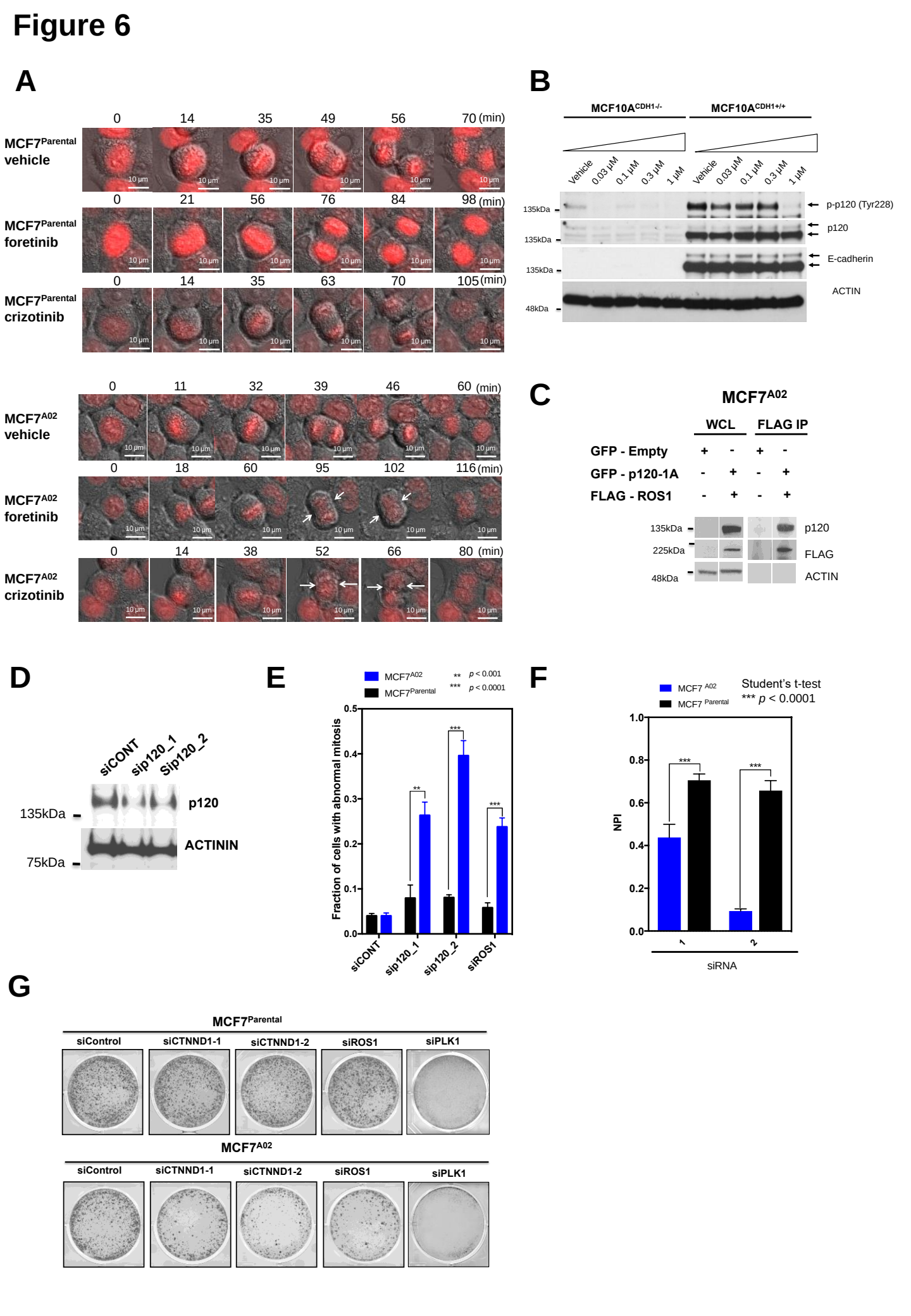
A
MCF7Parental vehicle
MCF7Parental foretinib
MCF7Parental crizotinib
MCF7A02 vehicle
MCF7A02 foretinib
MCF7A02 crizotinib
(min)
B
MCF10ACDH1-/-
MCF10ACDH1+/+
Vehicle
0.03 μM
0.1 μM
0.3 μM
1 μM
135kDa
48kDa
p-p120 (Tyr228)
p120
E-cadherin
ACTIN
C
MCF7A02
WCL
FLAG IP
GFP - Empty
GFP - p120-1A
FLAG - ROS1
135kDa
225kDa
48kDa
p120
FLAG
ACTIN
D
siCONT
sip120_1
Sip120_2
135kDa
75kDa
p120
ACTININ
E
MCF7A02
MCF7Parental
** p < 0.001
*** p < 0.0001
Fraction of cells with abnormal mitosis
siCONT
sip120_1
sip120_2
siROS1
F
MCF7 A02
MCF7 Parental
Student's t-test
*** p < 0.0001
NPI
siRNA
G
MCF7Parental
MCF7A02
siControl
siCTNND1-1
siCTNND1-2
siROS1
siPLK1

Figure 7

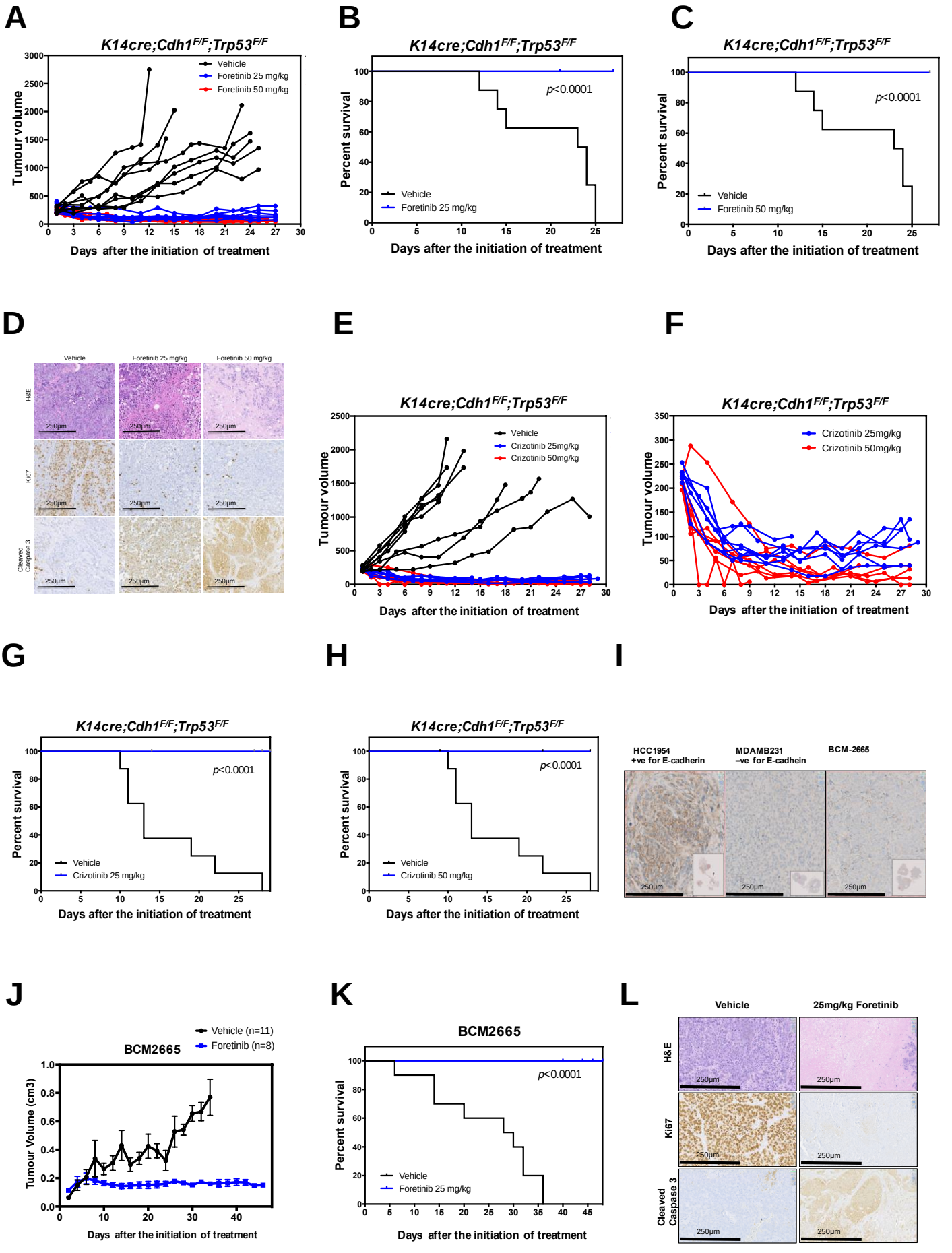
A
K14cre;Cdh1F/F;Trp53F/F
Vehicle
Foretinib 25 mg/kg
Foretinib 50 mg/kg
Tumour volume
Days after the initiation of treatment
B
K14cre;Cdh1F/F;Trp53F/F
p<0.0001
Vehicle
Foretinib 25 mg/kg
Percent survival
Days after the initiation of treatment
C
K14cre;Cdh1F/F;Trp53F/F
p<0.0001
Vehicle
Foretinib 50 mg/kg
Percent survival
Days after the initiation of treatment
D
Vehicle
Foretinib 25 mg/kg
Foretinib 50 mg/kg
H&E
Ki67
Cleaved Caspase 3
250μm
E
K14cre;Cdh1F/F;Trp53F/F
Vehicle
Crizotinib 25mg/kg
Crizotinib 50mg/kg
Tumour volume
Days after the initiation of treatment
F
K14cre;Cdh1F/F;Trp53F/F
Crizotinib 25mg/kg
Crizotinib 50mg/kg
Tumour volume
Days after the initiation of treatment
G
K14cre;Cdh1F/F;Trp53F/F
p<0.0001
Vehicle
Crizotinib 25 mg/kg
Percent survival
Days after the initiation of treatment
H
K14cre;Cdh1F/F;Trp53F/F
p<0.0001
Vehicle
Crizotinib 50 mg/kg
Percent survival
Days after the initiation of treatment
I
HCC1954
+ve for E-cadherin
MDAMB231
–ve for E-cadhein
BCM-2665
250μm
J
Vehicle (n=11)
Foretinib (n=8)
BCM2665
Tumour Volume (cm3)
Days after the initiation of treatment
K
BCM2665
p<0.0001
Vehicle
Foretinib 25 mg/kg
Percent survival
Days after the initiation of treatment
L
Vehicle
25mg/kg Foretinib
H&E
Ki67
Cleaved Caspase 3
250μm